PRELIMINARY AERODYNAMIC DESIGN CONSIDERATIONS FOR ADVANCED LAMINAR FLOW AIRCRAFT CONFIGURATIONS

Joseph L. Johnson, Jr., Long P. Yip, and Frank L. Jordan, Jr.
NASA Langley Research Center
Hampton, Virginia 23665

SUMMARY

Recent aerodynamic research on advanced aircraft configurations has revealed some important design considerations that affect aerodynamic efficiency and performance, stability and control, and safety of flight. Modern composite manufacturing methods have provided the opportunity for smooth surfaces that can sustain large regions of natural laminar flow (NLF) boundary-layer behavior and have stimulated interest in developing advanced NLF airfoils and improved aircraft designs. The present paper overviews some of the preliminary results obtained in exploratory research investigations on advanced aircraft configurations at the NASA Langley Research Center. Results of the initial studies have shown that the aerodynamic effects of configuration variables such as canard/wing arrangements, airfoils, and pusher-type and tractor-type propeller installations can be particularly significant at high angles of attack. Flow field interactions between aircraft components were shown to produce undesirable aerodynamic effects on a wing behind a heavily loaded canard, and the use of properly designed wing leading-edge modifications, such as a leading-edge droop, offset the undesirable aerodynamic effects by delaying wing stall and providing increased stall/spin resistance with minimum degradation of laminar flow behavior.

INTRODUCTION

In recent years, there have been significant performance improvements in general aviation aircraft from the realization of increased amounts of NLF (see refs. 1 through 8). This result was achieved in part through advanced NLF airfoil design and modern construction materials and fabrication techniques such as composites and milled or bonded aluminum skins. In addition, there have been design trends toward unconventional aircraft arrangements incorporating unusual features such as canards, tandem wings, and multiple surfaces to obtain performance gains. Preliminary results suggest that the use of some of these features provides weight savings, improved cabin layouts, and improved aerodynamic characteristics which can provide significant performance benefits and increased overall operating efficiency and utility. Examples of such advanced designs are the Gates Learjet/Piaggio GP-180, a three-surface configuration with twin-pusher engines mounted on the wing (fig. 1), and the Beech Aircraft Corporation Starship I, a canard configuration with twin-pusher engines mounted on the wing (fig. 2). Although the advanced aircraft designs with new

technology features and modern construction techniques appear very promising from performance considerations, information on the aerodynamic characteristics of unconventional configurations, particularly those with strong flow-field interactions, is very limited. For this reason, several recent system studies and wind-tunnel investigations have been initiated to provide a technology base for evaluating the aerodynamic characteristics of the advanced designs. The initial results of these wind-tunnel investigations indicate the importance of recognizing the strong aerodynamic interactions that can result from placing propulsion systems or control surfaces in unconventional locations.

Flow-field interactions between aircraft components can produce undesirable aerodynamic effects, and the use of wing leading-edge modifications may be required to offset the undesirable aerodynamic effects and improve stall/spin resistance. Preliminary results have shown that the application of a properly designed wing leading-edge droop to advanced NLF wings can improve the stall/spin resistance of these wings with minimum performance degradation. This paper presents some of the initial results of the exploratory aerodynamic investigations for several of the configurations investigated and discusses the significance of the results from overall performance and stability and control considerations.

SYMBOLS

b	wing span, ft
BL	butt line
C	canard
$\bar{c}$	wing mean aerodynamic chord, ft
c	local chord, ft
C_D	drag coefficient, Drag/qS
C_{D_c}	canard drag coefficient
C_L	lift coefficient, Lift/qS
C_{L_c}	canard lift coefficient, Canard lift/qS_c
C_{l_p}	roll damping
C_m	pitching-moment coefficient, Pitching moment/$q\bar{S}c$
C_{m_c}	canard pitching-moment coefficient
C_n	section normal-force coefficient, Normal force/qc
C_T	propeller thrust coefficient, Thrust/qS
ΔF_c	incremental force on canard due to power, lb
F_p	propeller normal force, lb
ΔF_w	incremental force on wing due to power, lb
LE	leading edge
q	dynamic pressure, lb/ft^2
R_N	Reynolds number
S	wing area, ft_2

S_c canard area, ft^2

WL water line

x local wing chord, ft

y lateral distance from wing centerline, ft

α angle of attack, deg

β sideslip angle, deg

δ_e elevator deflection, deg

Notation:

C.G. center of gravity

MODELS AND TEST CONDITIONS

The models used to provide aerodynamic information for discussion in this paper include the following configurations:

- Canard, single-engine pusher
- Canard, single-engine tractor
- Conventional single-engine tractor design
- Conventional business jet design
- Three-surface design
- Over-the-wing propeller design

The canard, pusher configuration was a full-scale model of a propeller-driven homebuilt aircraft which has demonstrated good performance and a high level of stall/spin resistance in operational use (see refs. 3 to 5). The canard, tractor configuration was a sub-scale model of an advanced general aviation design which incorporated a relatively close-coupled canard and an aft-mounted wing of relatively low sweep (see ref. 6). A single-slotted elevator on the canard provided pitch control. For the canard models, an auxilary balance was used to measure canard loads independently from the total aerodynamic loads measured on a main balance.

The conventional single-engine tractor model and the conventional business jet model represent configurations incorporating advanced NLF airfoils for improved performance (see refs. 7 and 8). One of the unique features of these configurations was the application of leading-edge droop designs which increased stall/spin resistance without significantly degrading NLF performance (see ref. 9). The three-surface design and the over-the-wing propeller design were configurations derived from a general purpose model used in generic studies to explore low-speed stability and control characteristics of advanced designs including the effects of power with aft-mounted engines (see refs. 10 and 11). The wind-tunnel results presented in this paper were obtained in investigations conducted in the Langley 30- by 60-Foot Wind Tunnel and 12-Foot Low-Speed Wind Tunnel.

RESULTS AND DISCUSSION

Canard, Single-Engine Pusher

Presented in figure 3 is a photograph of the large-scale canard, single-engine pusher configuration investigated in the Langley 30- by 60-Foot Wind Tunnel. The model was constructed with smooth fiberglass

surfaces and was equipped with pressure ports in the canard and wing to give detailed pressure distribution data. This investigation revealed many important design considerations for canard aircraft and pointed out the significance of these design features on performance, stability, and control characteristics (see refs. 4 and 5). Some of the more significant results of the investigation include: (1) the influence of the canard downwash on the wing aerodynamics; (2) the large regions of NLF on the smooth fiberglass surfaces; (3) the effect of canard airfoil section on stability and control; and (4) the effect of the engine location on propeller efficiency and stability and control. One of the most important, unexpected findings resulting from the wind-tunnel investigation was the discovery of large regions of NLF boundary-layer behavior. Using a sublimating chemical technique for transition visualization, it was determined that NLF existed back to 55-percent chord on the canard, 65-percent chord on the wing, and 60-percent chord on the winglets for a cruise attitude (see fig. 4). Figure 5 shows the flight vehicles which were used to verify the amount of NLF indicated in the wind-tunnel tests. Figure 5(c) shows the results of chemical sublimation tests conducted in flight and illustrates that the amount of NLF achieved in flight on the canard was similar to that measured in the wind tunnel (back to 55-percent chord station). As part of the 30- by 60-foot wind-tunnel investigation, tests were conducted to force premature boundary-layer transition on the canard by either carborundum grit applied at 5-percent chord or by water spray. These tests were initiated because of pilot reports of such aircraft experiencing a pitch trim change when entering rain. To determine whether this trim change was the result of early laminar to turbulent boundary-layer transition caused by rain, a test apparatus was used for rain simulation as shown in figure 6. The test apparatus consisted of a horizontal boom mounted in the wind tunnel about 4 chord lengths ahead of the canard. Results of the forced boundary-layer transition tests (presented in fig. 7) show that forced transition by either carborundum grit or rain simulation resulted in a significant reduction in the canard lift-curve slope and increased canard drag. Figure 8 shows that fixed boundary-layer transition on the canard caused, as expected on the basis of premature trailing-edge flow separation and reduced canard lift-curve slope, an increase in longitudinal stability and loss of elevator control effectiveness. These results point out the importance of airfoil selection to avoid changes in lift characteristics with loss of laminar flow. Advanced NLF airfoils have been designed to minimize the loss in lift due to premature transition (see ref. 7). Advanced NLF airfoils will be examined in more detail in subsequent sections of this paper.

Included in the investigation of canard airfoil design was a study of the effect of canard configuration on stall/post-stall behavior. Figure 9 shows the two airfoils investigated to illustrate the effects of camber and shape on stability and control. Presented in figure 10(a) are pitching-moment characteristics of the aircraft with the two different canards, and the data show significant differences in the stall/post-stall angle-of-attack range. For either airfoil configuration, the data show a stable

break at wing stall, but in the post-stall angle-of-attack range the NACA 0012 airfoil shows a marked destabilizing trend and positive pitching moments at high angles of attack. The significance of such a trend is that for certain landing conditions there may exist the possibility of inadvertently entering the post-stall angle-of-attack region and experiencing a deep-stall trim condition. The data of figure 10(b) show the importance of airfoil design in avoiding undesirable deep-stall characteristics. The significant point of figure 10(b) is that the GU25-5(11)8 airfoil has a relatively flat lift-curve slope following the stall, whereas the NACA 0012 airfoil shows an abrupt loss of lift at the stall and then an increase in lift in the post-stall angle-of-attack range. The increase in canard lift-curve slope in the post-stall angle-of-attack range is very destabilizing because an increase in canard lift tends to aggravate the destabilizing effect of wing stall on pitch stability for a canard arrangement. The stability and control of canard arrangements will be discussed in further detail in the section of this paper dealing with tractor engine arrangements.

Figure 11 presents a sketch to introduce the subject of canard downwash and vortex-wake interaction effects on the main wing. The two main points to be discussed are the canard downwash on the inboard portion of the wing, and the canard vortex flow which introduces an upwash on the wing tip. Figure 12 presents measured section normal-force coefficient data to show the effect of the canard wake on the wing and indicates, as expected, that a reduction in span loading occurs inboard and an increase in span loading occurs at the wing tip. The results of tuft flow studies (fig. 13(a)) show that the aircraft experiences spanwise flow on the wing and severe tip stall at $\alpha = 19.5°$. The use of a leading-edge droop, shown in cross section in figure 13(b), is shown by the tuft photograph of figure 13(a) to provide attached flow at the wing tip.

The importance of wing leading-edge treatment for swept wings is illustrated in a plot of aspect ratio against wing sweep in figure 14. The figure was taken from reference 12 and shows that swept wings with high aspect ratios tend to have an unstable pitching-moment break at the stall due to tip stall. The figure does not take into account the effects of such items as winglets or canard vortex flow on the wing tip stall. Such effects emphasize the need for additional research on the use of wing leading-edge treatment for improved stall characteristics. Figure 15 shows the stabilizing effect of the wing leading-edge droop on the pitching-moment characteristics of the canard single-engine pusher configuration, and figure 16 shows the stabilizing effect of the leading-edge droop on roll damping. Model and airplane flight tests verified the damping-in-roll data of figure 16 and showed that the wing leading-edge droop eliminated a wing rock tendency of the basic airplane configuration for aft center-of-gravity location.

Canard, Single-Engine Tractor

Discussion of the canard, single-engine tractor configuration emphasizes the effects of canard airfoil section

and the effects of power on longitudinal stability characteristics. More complete discussion of the overall stability and control characteristics of the tractor configuration is presented in reference 6.

Presented in figure 17 is a photograph of the canard, tractor model mounted for static wind-tunnel tests in the Langley 30- by 60-Foot Wind Tunnel. The model has a closely coupled canard-wing arrangement with the canard placed slightly above the wing. Power for the subject model was supplied by a tip-turbine air motor driven by compressed air.

Figure 18 shows a comparison of the effects of power on the pitching-moment characteristics of the canard, tractor and pusher configurations for climb power (C_T = 0.4) and aft center-of-gravity conditions. The data show that the power effects were destabilizing for the tractor model and stabilizing for the pusher model. The large nose-up trim changes for the tractor model were caused by a combination of direct propeller normal force and induced effects on the canard and wing. As indicated in the sketch of figure 18, the rearward location of the propeller results in a propeller normal force which produces a nose-down or stabilizing pitching moment.

Figure 19 shows the effect of canard airfoil section on the pitching-moment characteristics of the tractor configuration. Of particular interest in figure 19 is the relative difference between the pitching-moment data of the NACA 23018 airfoil and two NLF airfoils, the GU25-5(11)8 and the NLF(1)-0416, in the post-stall angle-of-attack range. As noted in the preceding section, the post-stall stability characteristics of canard configurations can be greatly influenced by the canard airfoil. For the three airfoils investigated, the NACA 23018 gives the most destabilizing pitching-moment trends at post-stall angle of attack. The reason for this trend is that the NACA 23018 is a relatively thin airfoil which exhibits a sharp stall and an increase in lift-curve slope at post-stall angles of attack and becomes very destabilizing. The other airfoils of figure 19 tend to have a relatively flat lift curve at stall and, therefore, give more desirable post-stall stability contributions.

As part of the exploratory research on the tractor design, tests were continued to examine in more detail the aerodynamic characteristics of the GU25-5(11)8 and the NLF(1)-0416 airfoils. Presented in figure 20 are the results of some of the exploratory tests to show the effect of Reynolds number, and presented in figure 21 are the effects of forced boundary-layer transition using carborundum grit applied at the 5-percent chord station. The significant results of figures 20 and 21 are that the aerodynamic characteristics of the NLF(1)-0416 are not sensitive to Reynolds number or forced boundary-layer transition; whereas, the GU25-5(11)8 airfoil shows loss of canard lift due to boundary-layer separation at low Reynolds number and, also, loss of lift due to forced boundary-layer transition. The NLF(1)-0416 airfoil aerodynamic characteristics are typical of several advanced NLF airfoils developed in recent years which provide promising performance gains. Application of some of the advanced NLF airfoils to conventional airplane

configurations for improved performance will be addressed in subsequent sections.

Included in the canard, tractor investigation were tests to study the effect of relative locations of the canard and wing on longitudinal characteristics of the configuration. Presented in figure 22 is a photograph of the tractor model with the canard lowered on the fuselage and the wing raised to the top of the fuselage. The data of figure 23 show that modifying the configuration to have the canard lowered and the wing raised provided a stabilizing influence on longitudinal stability in the post-stall angle-of-attack range and eliminated the undesirable deep-stall tendency of the basic configuration with power on. The stabilizing effect of the modified design apparently results from moving the canard out of the propeller slipstream and moving the wing out of the canard downwash.

Conventional Single-Engine Tractor Design

The discussion of conventional configurations will emphasize the use of advanced NLF airfoils for improved performance and the application of wing leading-edge droop to the NLF airfoils to improve stall/spin resistance with minimum performance degradation. Before discussing the new airfoil configurations, a brief review of related stall/spin research at Langley is provided to discuss the development of an effective wing leading-edge droop for increased departure resistance.

Shown in figure 24 are the research airplanes flown at Langley in the stall/spin research program. These research airplanes were flown with a modified wing leading-edge droop which proved effective for increased stall/spin resistance. Figure 25 shows some design features of the droop arrangement developed for the T-tail research airplane. An important feature of the droop is the abrupt discontinuity of the droop inboard leading-edge. This discontinuity is effective in generating a vortex which acts as an aerodynamic fence to stop the spanwise flow from the inboard portion of the wing as stall progresses. The leading-edge droop extends to near the wing tip such that the outer position of the wing performs as a low-aspect-ratio wing with a very high stall angle of attack. Flow visualization studies using fluorescent oil provide an excellent means of illustrating the effectiveness of the leading-edge droop. Figure 26 presents the results of oil flow studies and shows the basic wing in a stalled condition with a predominant outward flow direction. The outboard droop is shown to keep the outer wing panel flow attached to $\alpha = 35°$. A summary of the effectiveness of the droop for spin prevention is presented in figure 27 which shows that the leading-edge droop significantly improved the spin resistance of the research airplanes.

The recent trend in general aviation airplane design toward the use of NLF airfoils for improved performance has led to an interest in applying the wing leading-edge technology developed in stall/spin research to the new NLF airfoils. Two NLF airfoils of current interest are the NLF(1)-0215F and the NLF(1)-0414F (see fig. 28). One approach recently studied in exploratory research programs at Langley was to use the NLF(1)-0414F airfoil for enhanced performance, and the NLF(1)-0215F

airfoil for the droop required for improved spin resistance. A leading-edge droop was developed from the NLF(1)-0215F airfoil by gloving over the leading-edge outboard panel of the wing. Presented in figure 29 is a sketch of the advanced wing planform, compared to the planform of a more conventional general aviation wing. The advanced wing is of higher aspect ratio, and the droop is smaller in span and located further outboard than that derived for conventional wings in earlier research. The droop was developed in subscale tests in the Langley 12-Foot Low-Speed Wind Tunnel using a wing-tip balance to measure the aerodynamics of the outer wing panel. This research also revealed that the effectiveness of the outboard droop could be enhanced by the addition of a small-span inboard droop located inboard on the wing. A photograph of the model used in the 12-foot tunnel test is presented in figure 30. The final droop geometry developed from the low-speed tests evolved from a number of exploratory studies of different designs. The fact that the most effective location of the droop was relatively far outboard on the wing is probably related to the stall pattern of the higher aspect ratio wing compared to that of previous wings investigated. Some oil flow studies conducted by Professor Allen Winkelman at the University of Maryland have shown that considerable differences occur in the stall behavior of wings of various aspect ratios. For example, presented in figure 31 are results of oil flow studies which show that in separated flow conditions the higher aspect ratio wings tend to have a greater number of stall cells on the wing trailing edge than noted for the lower aspect ratio wings. These differences in surface patterns between wings of different aspect ratio may be one of the reasons for different leading-edge droop requirements as the wing aspect ratio increases. Additional tests are planned to provide research information for use in wing leading-edge droop design for the advanced wing planform. Presented in figure 32 are the results of chemical sublimation tests conducted on a larger scale model of the general aviation advanced wing configuration. Figure 32 shows that the wing had NLF back to about 70-percent chord where transition occurred near the point of minimum pressure. Except for wedges along the edges of the droop, NLF also occurred behind the droop to the 70-percent chord station. Chemical sublimation tests on the lower side of the wing also showed NLF to about the 70-percent chord station. Thus, incorporation of the droop had a minimal impact on the character of the NLF features of the advanced wing.

The results of roll damping tests on the advanced wing, presented in figure 33, show that the leading-edge droop arrangement investigated eliminated the unstable roll damping at the stall for the basic wing and provided stable roll damping for the modified wing over the test angle-of-attack range.

Conventional Business Jet Design

Another configuration employing NLF airfoils for improved performance is the business jet shown in figure 34. The wing NLF airfoil used on the configuration is shown in figure 35. This airfoil is the NLF(1)-0414F and has the departure resistant leading-edge droop developed from the NLF(1)-0215F in a similar manner to that

discussed earlier for the advanced NLF wing on the general aviation research aircraft.

In order to determine the effectiveness of the wing leading-edge droop for departure resistance, damping-in-roll tests were made of the business jet configuration, and the results of the tests are presented in figure 36. The data of figure 36(a) show that the damping-in-roll characteristics of the basic wing became unstable near the stall angle of attack, and as the angle of attack increased, a region of stable damping developed and then the damping became unstable again near $\alpha = 35^{\circ}$. The addition of the outboard droop is shown to have eliminated the unstable damping near the stall. Although the configuration was not very heavily damped in the stall angle-of-attack range, the configuration would be expected to show increased departure resistance over that of the basic design. In an attempt to increase the roll damping of the configuration at the initial stall angle of attack, the basic leading-edge droop arrangement was modified to add a small inboard droop segment in combination with the outboard segment (see fig. 36(b)). This segmented droop arrangement was developed for the general aviation research configuration discussed in the preceding section. The data of figure 36(b) show that the modified droop arrangement provided a substantial increase in roll damping at the initial wing stall and provided good roll damping over the test angle-of-attack range. Figure 37 shows the results of chemical sublimation tests of the wing and modified leading-edge droop arrangement. The results show that NLF was maintained relatively far rearward on the wing chord (about 70-percent chord) and was not adversely affected by the wing leading-edge droop. Similar results were obtained for sublimation tests made on the bottom of the wing, indicating that performance penalties associated with the departure resistant wing should be small.

Three-Surface Configuration

Three-surface configurations employing NLF airfoils were recently investigated in exploratory studies at the Langley Research Center. Figure 38 shows plan views of the three-surface designs investigated and also a plan view of a conventional design tested to provide data for comparison purposes. Included in the study were configurations with aft-mounted engines and with wing-mounted pusher engines. All three configurations were derived from the basic model components. The model was equipped with a six-component strain-gage balance for measuring the total aerodynamic characteristics of the configuration and also had separate balances on the wing, canard, and the engine nacelle. More complete model descriptions are presented in reference 10. A photograph showing the model with aft-mounted engines is presented in figure 39. A comparison of the aerodynamic characteristics of the aft-mounted engine configurations with those of the conventional design is shown in figure 40. The lift data of figure 40(a) show a slightly higher lift-curve slope and maximum lift coefficient for the three-surface designs than for the conventional design. This result can be attributed to the lift of the canard and also to the fact that wing-nacelle interference effects of the conventional design were eliminated or minimized in the aft-mounted engine configurations.

The data of figure 40(b) show the effects of power on the longitudinal stability characteristics of the test configurations. Although all three configurations exhibited a pitch-up tendency, which is generally characteristic of a T-tail design, the three-surface configuration tended to have more aggravated pitch-up characteristics. This result can be attributed to the aft location of the wing in the three-surface design, which results in the wing giving relatively large destabilizing pitching-moment changes when the wing stalls. The data of figure 40(b) show a destabilizing effect of power on the longitudinal stability characteristics of the conventional design, whereas a significant stabilizing change in pitching moment due to power is shown for the three-surface configuration with aft-fuselage-mounted engines. Lateral-directional stability tests in sideslip showed that power effects were also very stabilizing characteristics for the aft-mounted engine arrangement.

Over-the-Wing Propeller Design

Presented in figure 41 is a photograph of an advanced configuration recently investigated which uses the propellers in an over-the-wing arrangement to induce large favorable interference effects of the propeller slipstream on the wing for reduced wing drag at high power settings (see ref. 10). This concept, which is based on earlier research with jet-engine aircraft, was derived from the three-surface design shown in figure 38 by rotating the engine nacelles and propellers from the pusher arrangement to the over-the-wing tractor arrangement. The drag data obtained with the over-the-wing propeller arrangement show that the drag of the wing decreases as the propeller thrust coefficient is increased. At the thrust coefficient corresponding to the climb condition, the drag of the wing relative to that for the power-off condition is significantly reduced. Preliminary results of tests to measure the effects of the wing proximity on the propeller efficiency indicated relatively small interference penalties on the propeller performance.

Additional tests with the over-the-wing propeller arrangement are currently planned using a forward-swept arrangement (fig. 42). The forward-swept wing configuration has the advantage of locating the wing root chord and over-the-wing propellers aft on the fuselage for improved structural efficiency and reduced cabin noise. Preliminary results with the forward-swept wing configuration indicate similar performance improvements for the over-the-wing propeller concepts to those determined earlier for straight-wing configurations. Preliminary stability and control studies indicate, however, that careful consideration must be given to tailoring of the forward-swept wing design to minimize pitch-up tendencies associated with early wing root stall and lateral instability (loss of effective dihedral) inherent with forward-swept wings. Follow-on tests at larger scale are planned to provide information for analysis and evaluation of over-the-wing propeller concept and forward-swept wing design at higher Reynolds numbers.

CONCLUDING REMARKS

The results of recent aerodynamic research on advanced configurations

have revealed some important design considerations that affect aerodynamic efficiency and performance, stability and control, and safety of flight. Modern composite manufacturing methods have provided large regions of NLF boundary-layer behavior and stimulated interest in developing advanced NLF airfoils and improved aircraft design. Experiments have indicated that selection of canard airfoils can be extremely important to avoid large pitch trim and stability changes between conditions of natural and forced turbulent boundary-layer transition; the canard airfoil characteristics at stall/post-stall angles of attack can determine the susceptibility of an aircraft to pitch-up and deep-stall trim problems. Flow-field interactions between aircraft components were shown to produce undesirable aerodynamic effects on a wing located behind a heavily loaded canard. The use of properly designed wing leading-edge modifications, such as a leading-edge droop, was found to delay wing stall and provide increased stall/spin resistance with minimum performance degradation. Power effects were shown to be generally stabilizing for aft-mounted engine arrangements and destabilizing for tractor-engine arrangements.

REFERENCES

1. Holmes, Bruce J.; Obara, Clifford J.; and Yip, Long P.: Natural Laminar Flow Experiments on Modern Airplane Surfaces. NASA TP-2256, June 1984.

2. Holmes, B. J.; and Obara, C. J.: Observations and Implications of Natural Laminar Flow on Practical Airplane Surfaces. ICAS Paper 82-5.1.1, 1982.

3. Rutan, B.: Development of a Small, High Aspect Ratio Canard Aircraft. Society of Experimental Test Pilots Technical Review, Vol. 13, No. 2, 1976, pp. 93-101.

4. Yip, L. P.; and Coy, P. F.: Wind Tunnel Investigation of a Full-Scale Canard-Configured General Aviation Aircraft. ICAS Paper No. 82-6.8.2, 1982.

5. Yip, Long P.: Wind-Tunnel Investigation of a Full-Scale Canard-Configured General Aviation Airplane. NASA TP-2382, 1985.

6. Chambers, Joseph R.; Yip, Long P.; and Moul, Thomas M.: Wind Tunnel Investigation of an Advanced General Aviation Canard Configuration. NASA TM-85760, April 1984.

7. Somers, Dan M.: Design and Experimental Results for a Natural-Laminar-Flow Airfoil for General Aviation Applications. NASA TP-1861, 1981.

8. Viken, Jeffrey K.: Aerodynamic Design Considerations and Theoretical Results for a High Reynolds Number Natural Laminar Flow Airfoil. M.S. Thesis, George Washington University, January 1983.

9. Staff of the Langley Research Center: Exploratory Study of the Effects of Wing Leading-Edge Modifications on the Stall/Spin Behavior of a Light General Aviation Airplane. NASA TP-1589, 1979.

10. Johnson, J. L., Jr.; and White, E. R.: Exploratory Low-Speed Wind-Tunnel Investigation of Advanced Commuter Configurations Including an Over-the-Wing Propeller Design. AIAA Paper 83-2531, October 1983.

11. Williams, L. J.; Johnson, J. L., Jr.; and Yip, L. P.: Some Aerodynamic Considerations for Advanced Aircraft Configurations. AIAA Paper 84-0562, 1984.

12. Shortal, Joseph. A.; and Maggin, Bernard.: Effect of Sweepback and Aspect Ratio on Longitudinal Stability Characteristics of Wings at Low Speeds. NACA TN-1093, 1946.

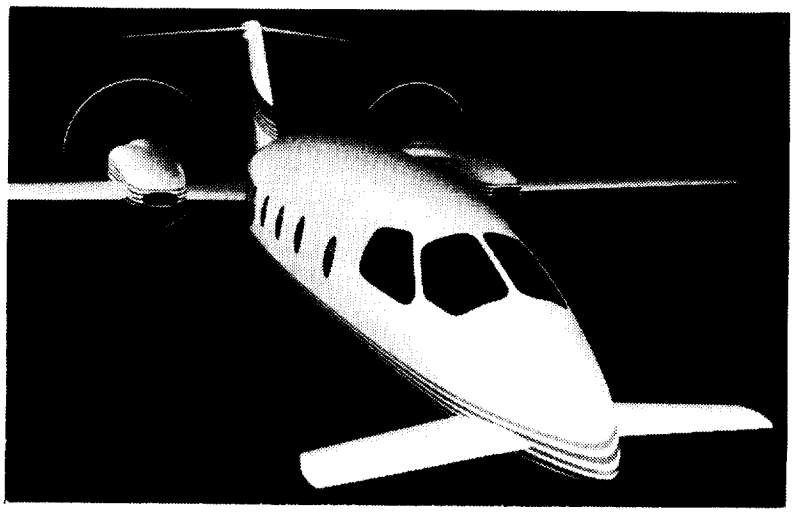

Figure 1.- Learjet/Piaggio GP-180.

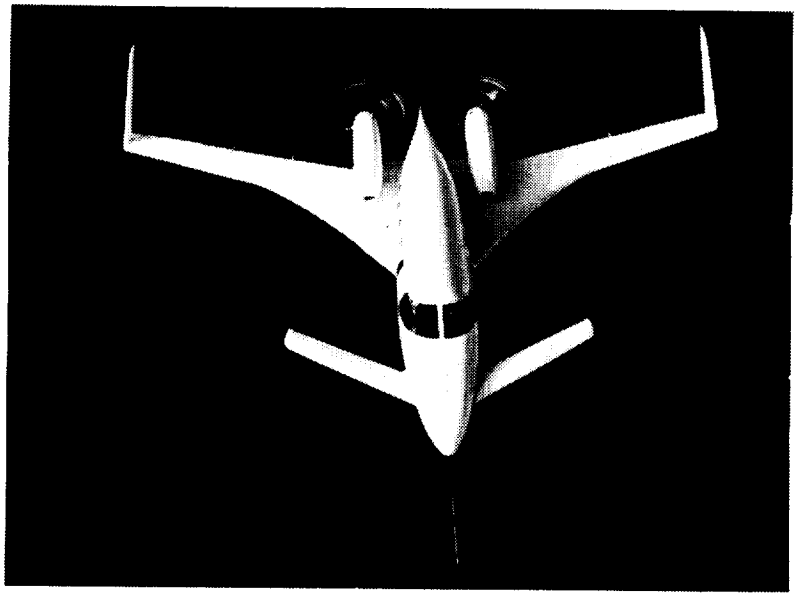

Figure 2.- Beechcraft Starship 1, 85-percent-scale flying prototype.

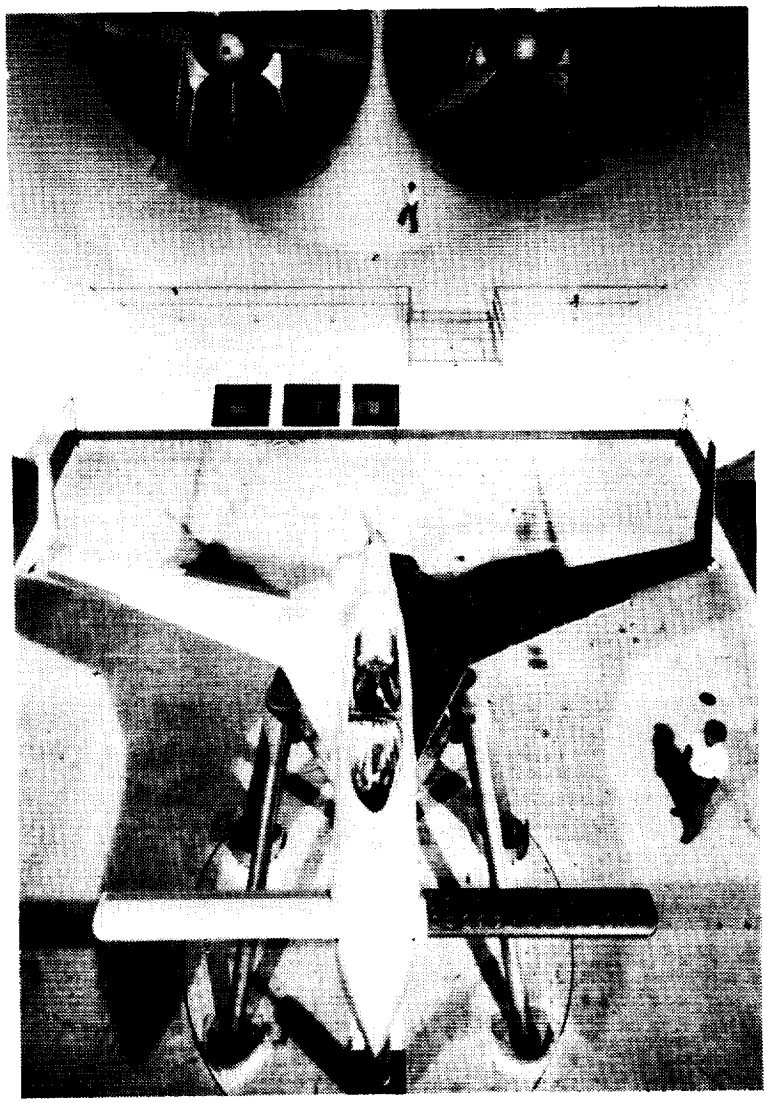

Figure 3.- Canard, single-engine pusher configuration in the Langley 30- by 60-Foot Wind Tunnel.

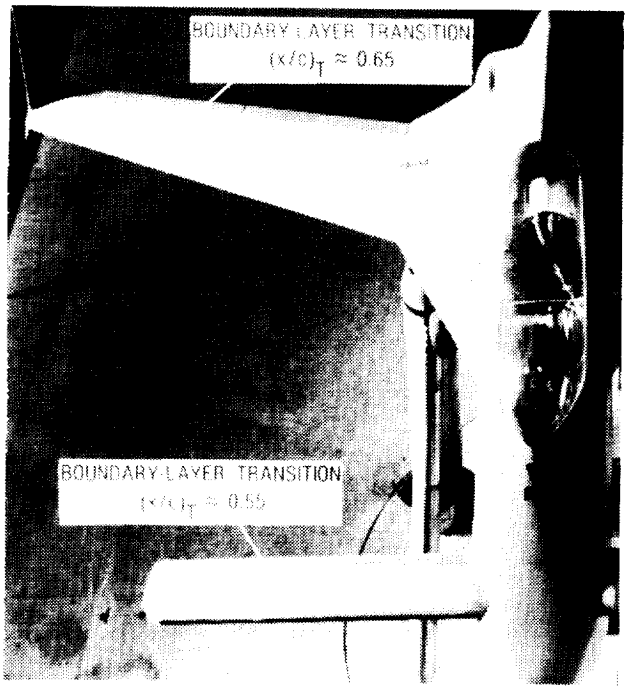

(a) Top view of wing and canard.

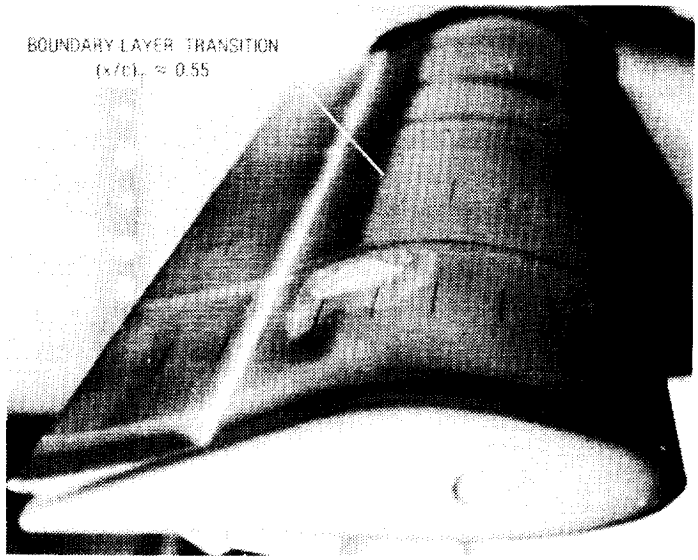

(b) Canard.

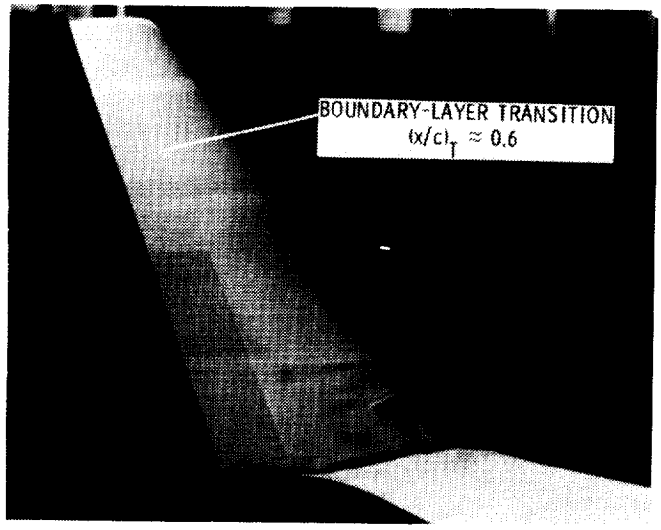

(c) Winglet.

Figure 4.- Flow visualization using sublimating chemicals to show boundary-layer transition.

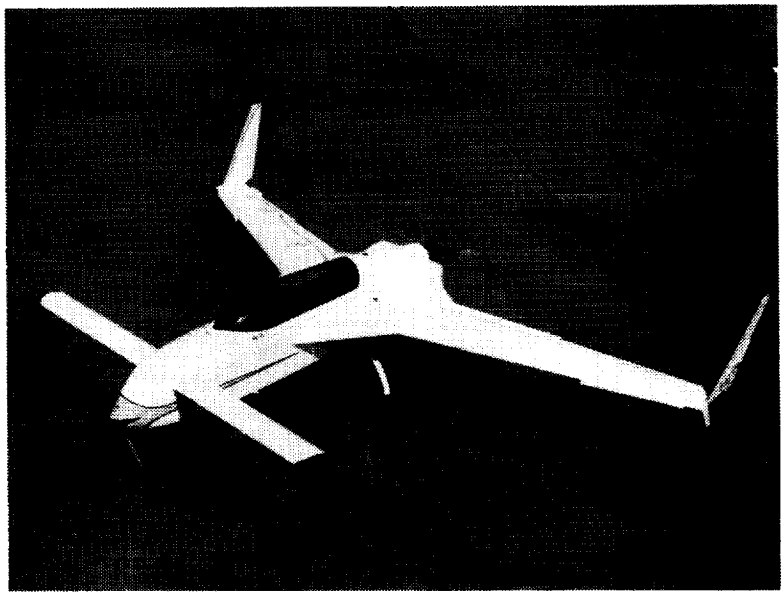

(a) Rutan Vari-eze.

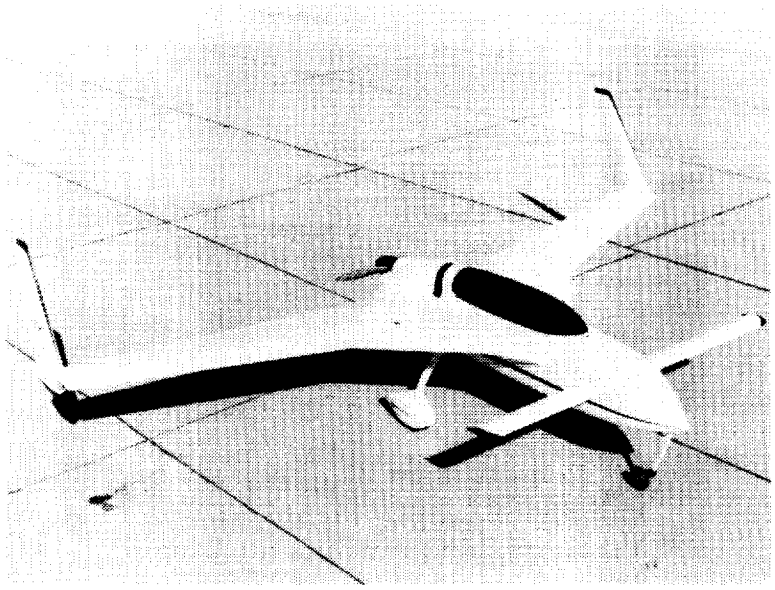

(b) Rutan Long-EZ.

Figure 5.- Canard, single-engine pusher airplanes used for natural laminar flow flight experiments.

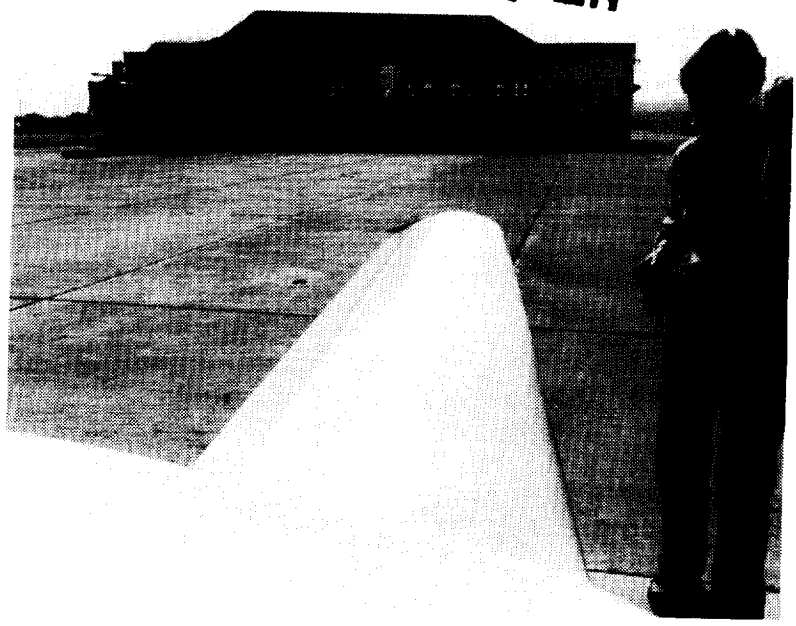

(c) Canard.

Figure 5.- Concluded.

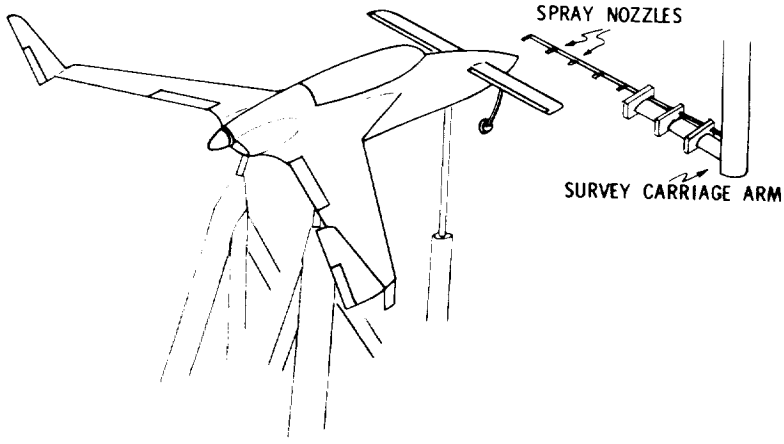

Figure 6.- Sketch of rain-simulation apparatus.

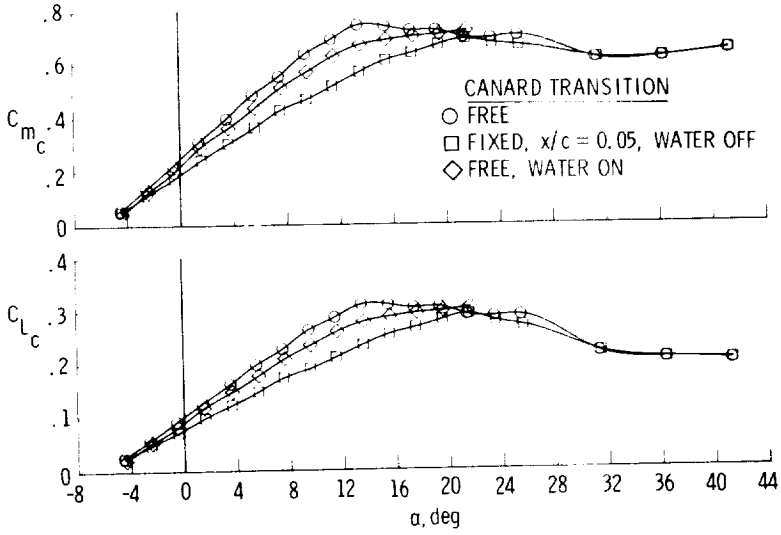

(a) Lift and pitching moments.

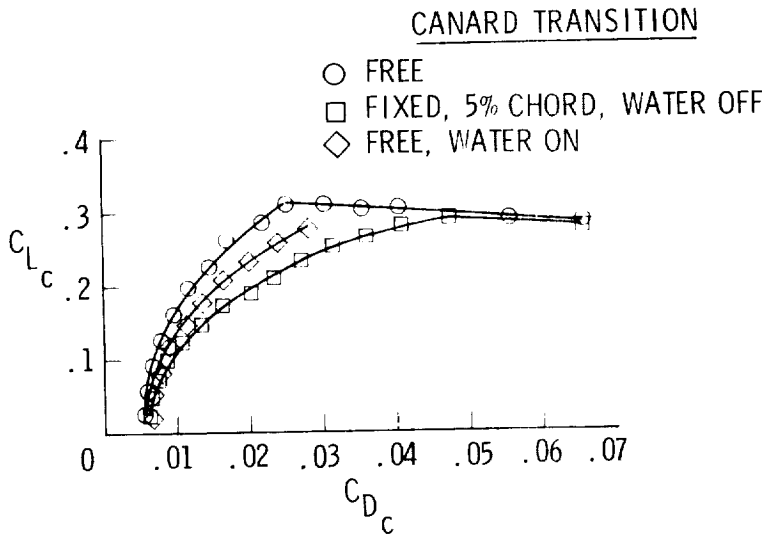

(b) Drag characteristics.

Figure 7.- Effect of water spray on canard aerodynamics.

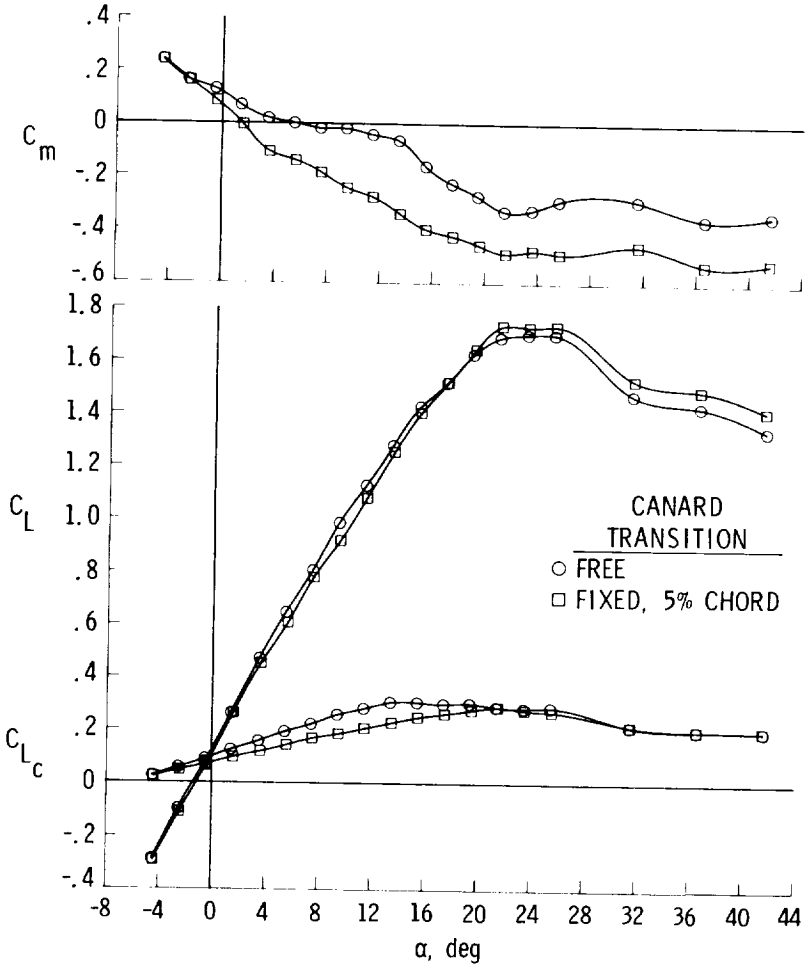

(a) Lift and pitching moments.

Figure 8.- Effect of canard transition on airplane aerodynamics.

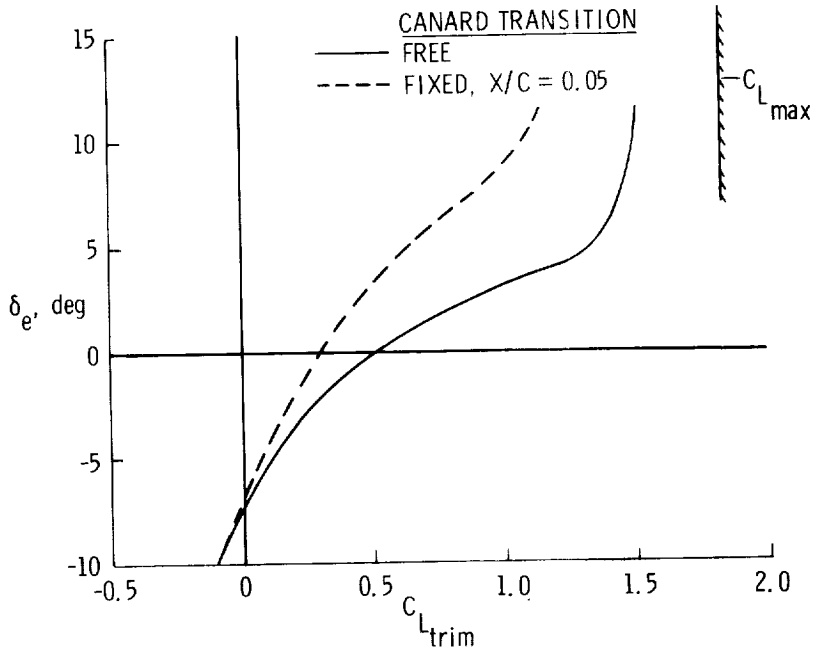

(b) Elevator effectiveness.

Figure 8.- Concluded.

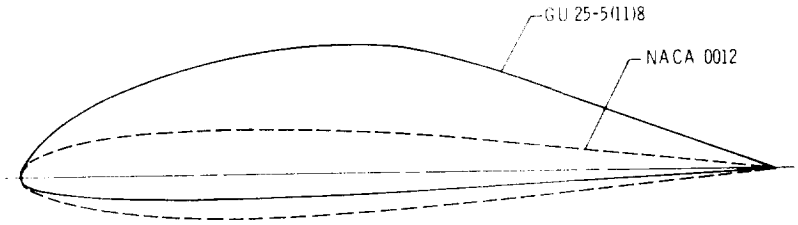

Figure 9.- Canard airfoil contours.

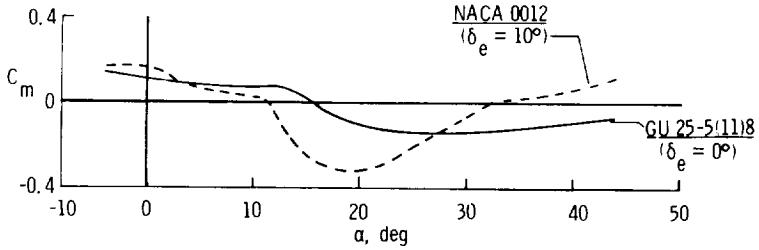

(a) Total pitching-moment characteristics.

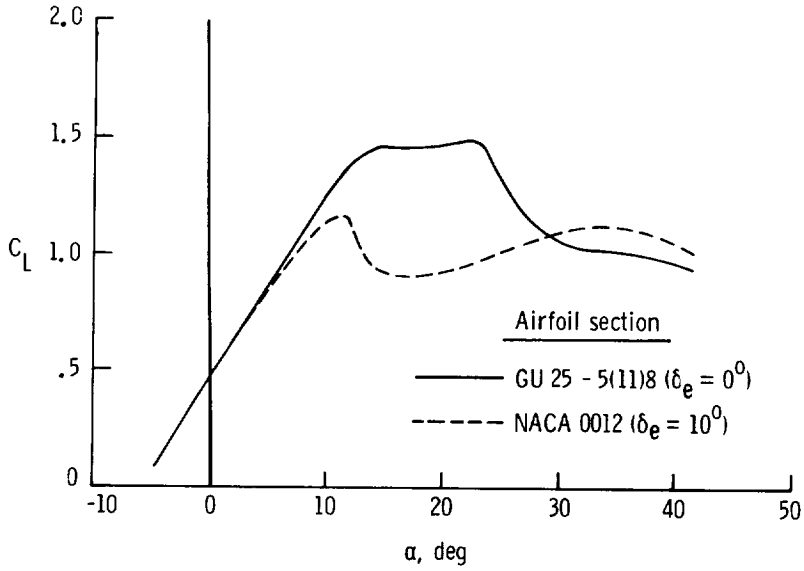

(b) Canard lift characteristics.

Figure 10.- Effect of canard on longitudinal stability of configuration with aft c.g.; Reynolds number = 1.60 million.

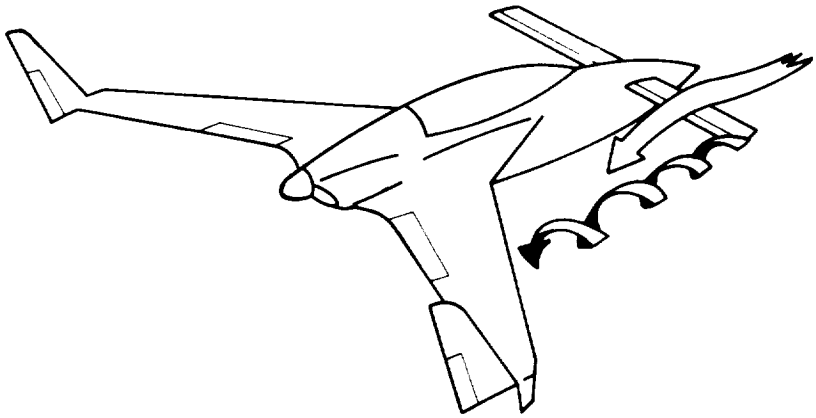

Figure 11.- Sketch of canard-wing aerodynamic flow interactions.

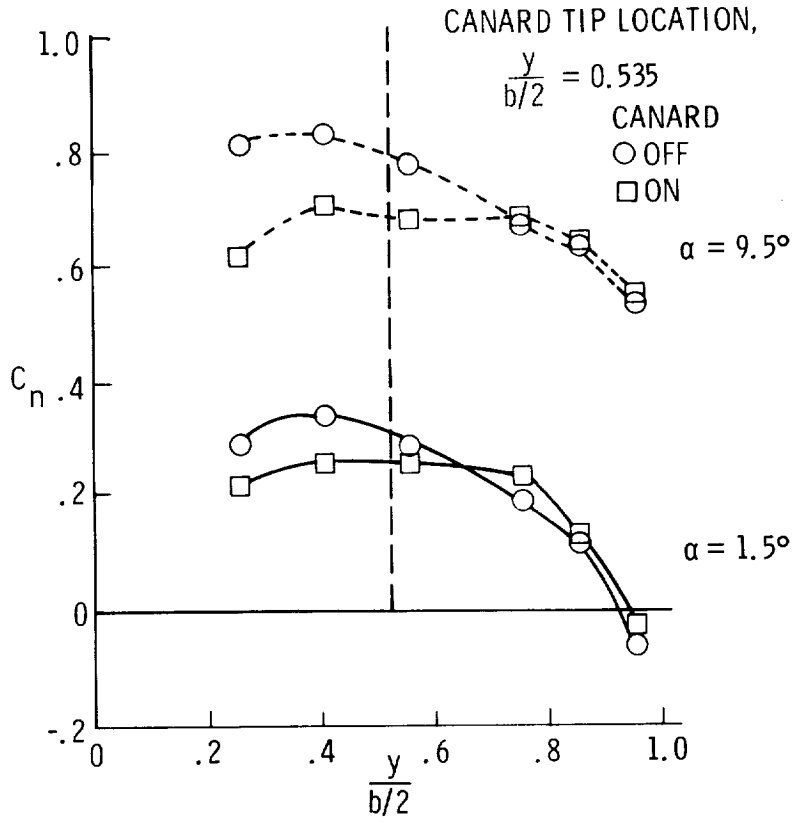

Figure 12.- Effect of canard on spanload distribution of wings.

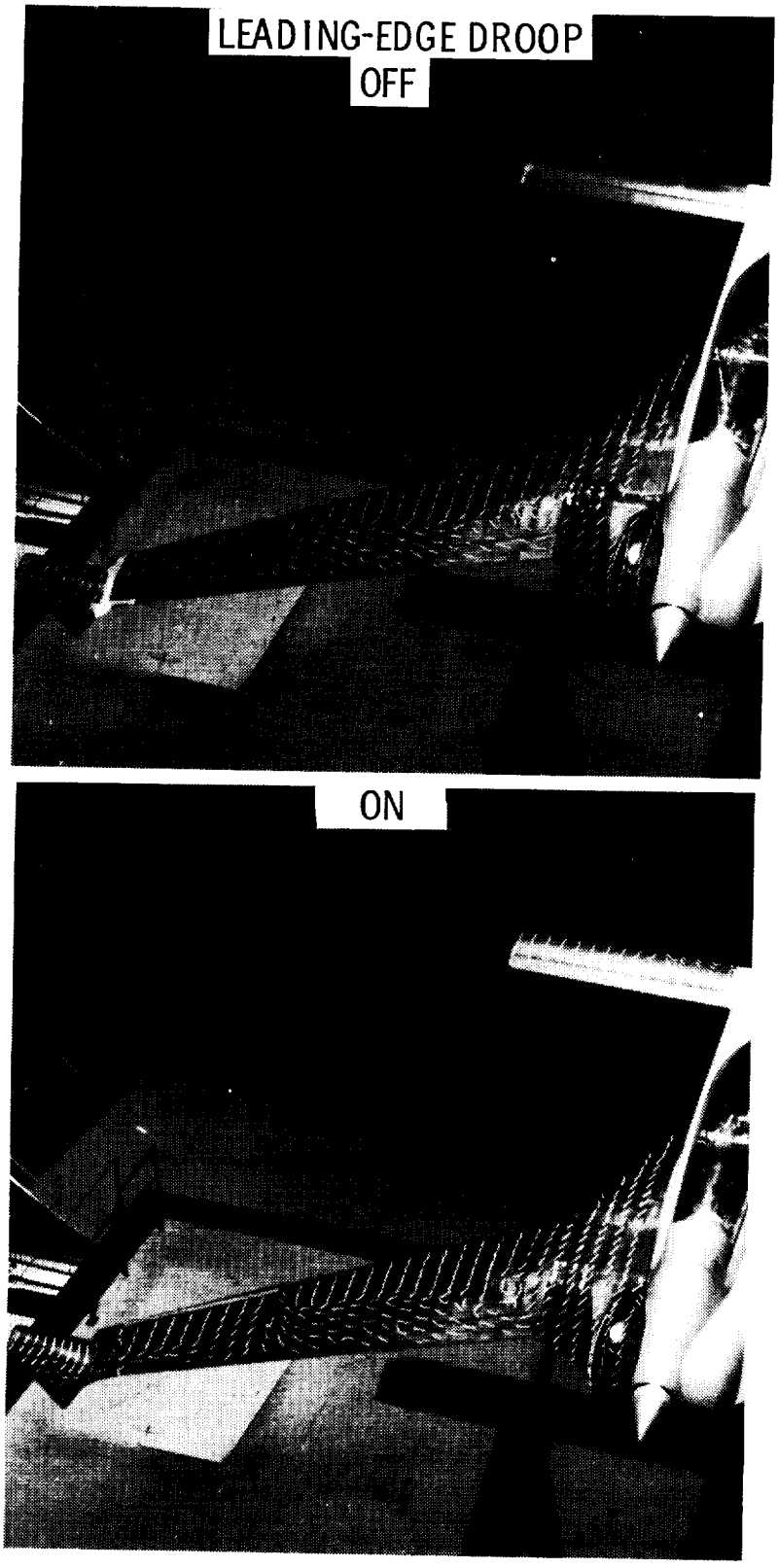

(a) Tuft flow visualization.

Figure 13.- Effect of leading edge on wing stall patterns, α = 19.5°.

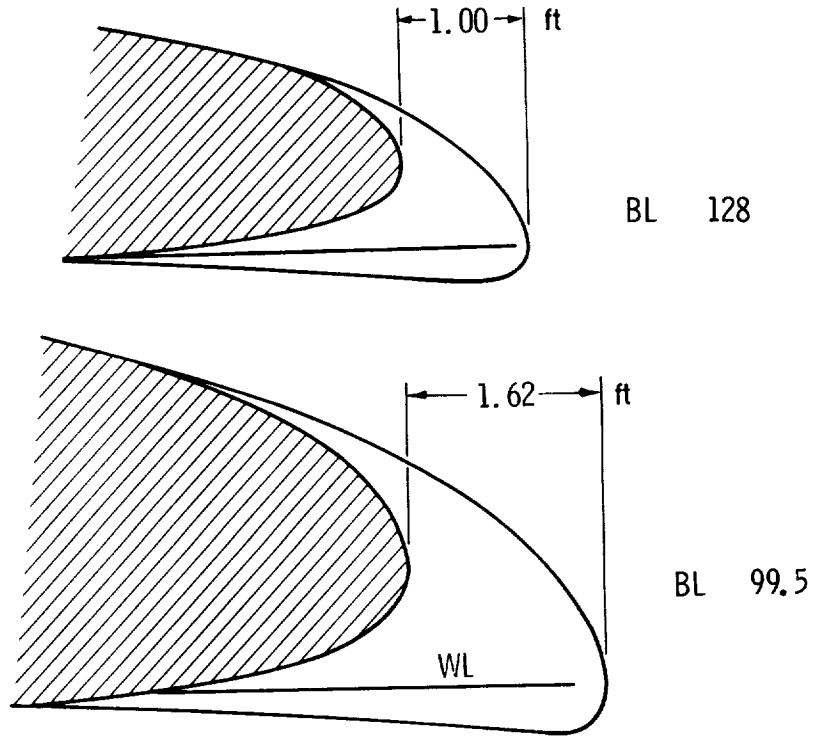

(b) Leading-edge droop.

Figure 13.- Concluded.

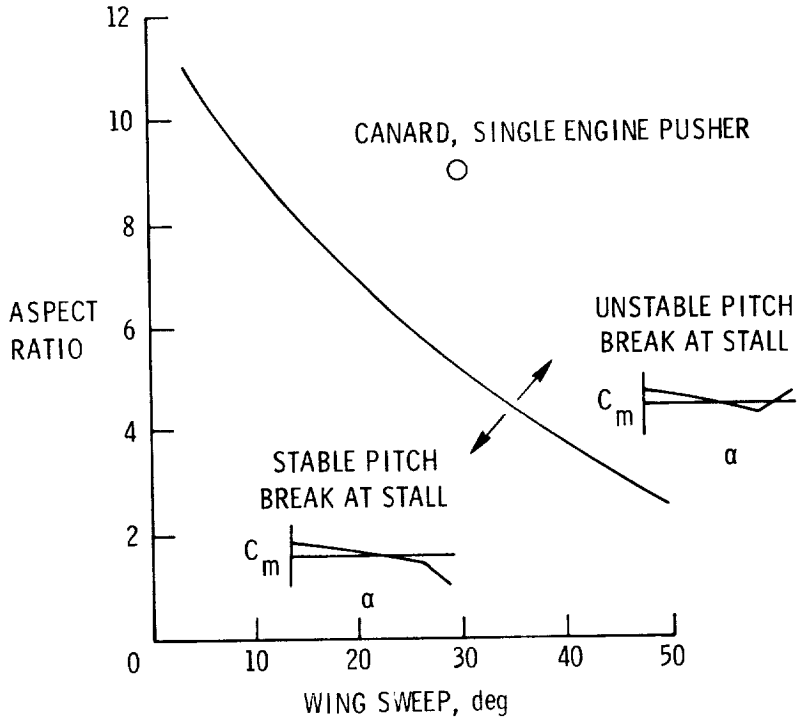

Figure 14.- Effect of wing aspect ratio and sweep on pitching-moment characteristics at stall.

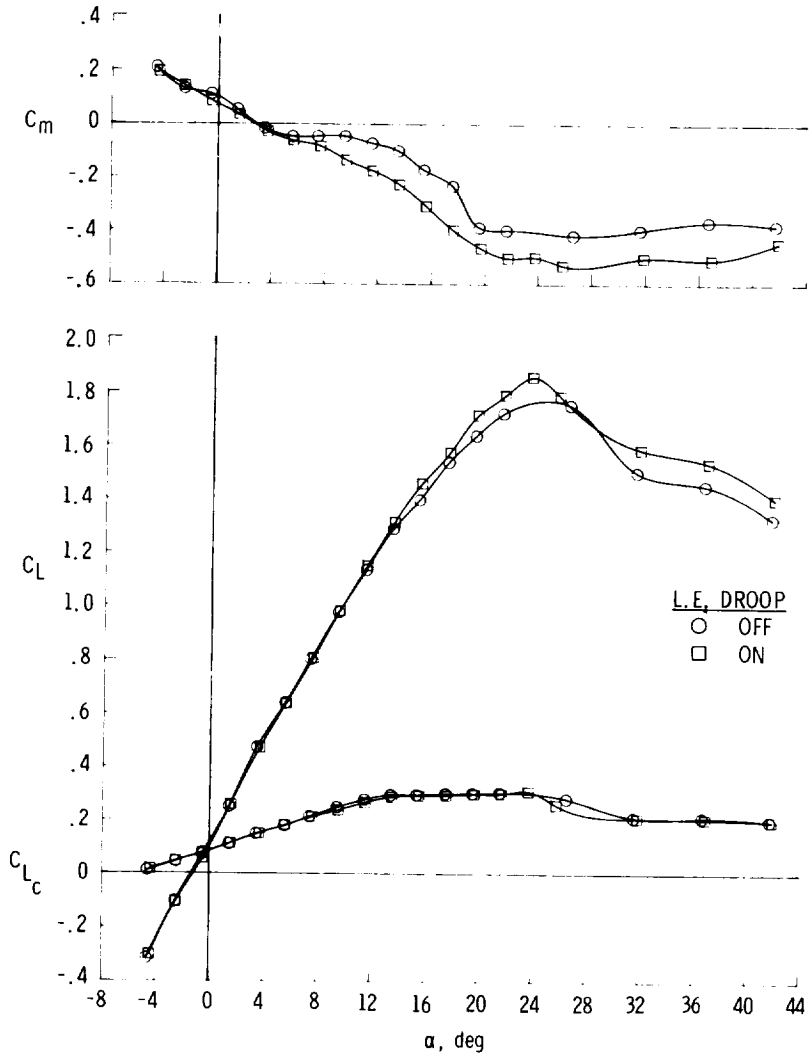

Figure 15.- Effect of leading-edge droop on longitudinal characteristics.

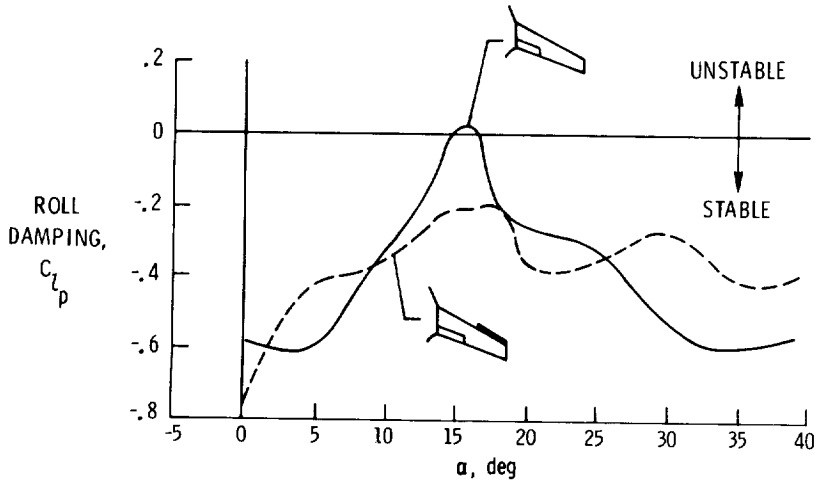

Figure 16.- Effect of leading-edge droop on roll damping characteristics.

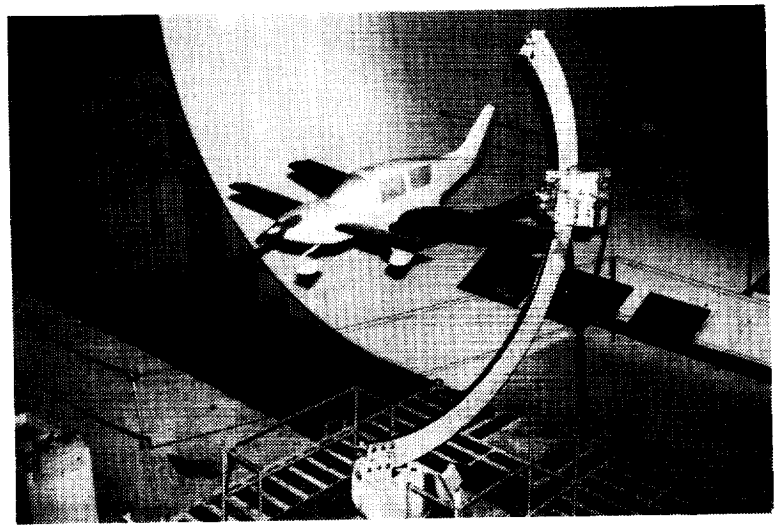

Figure 17.- Canard, tractor configuration mounted in the 30- by 60-Foot Wind Tunnel.

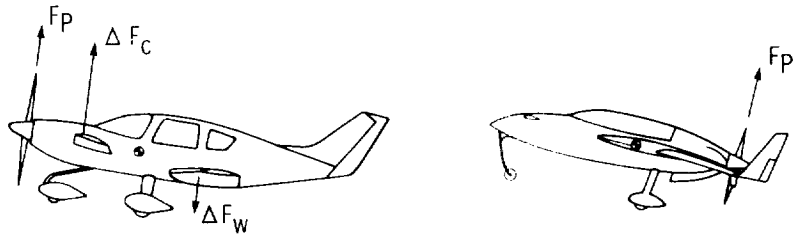

Tractor design
- Destabilizing effect

Pusher design
- Stabilizing effect

(a) Illustration of power effects.

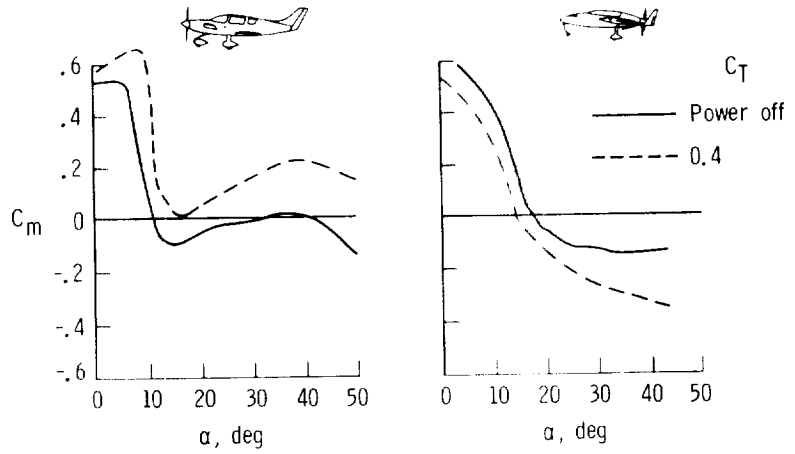

(b) Pitching-moment characteristics.

Figure 18.- Comparison of power effects on pitching-moment characteristics of canard tractor and pusher designs.

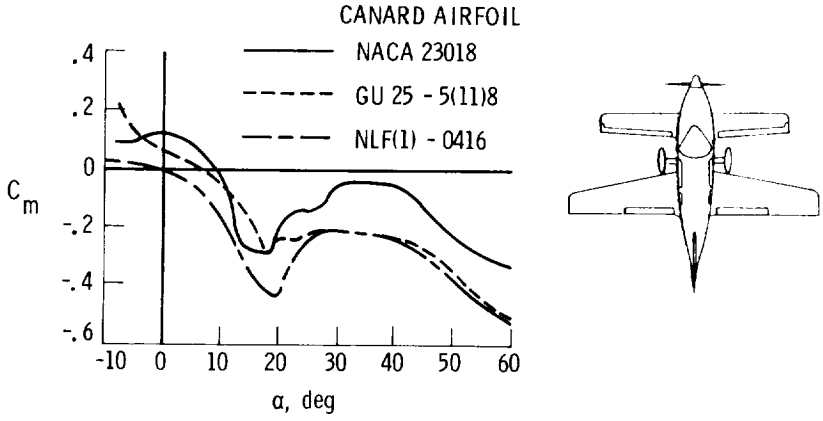

Figure 19.- Effect of canard airfoil on pitching-moment characteristics.

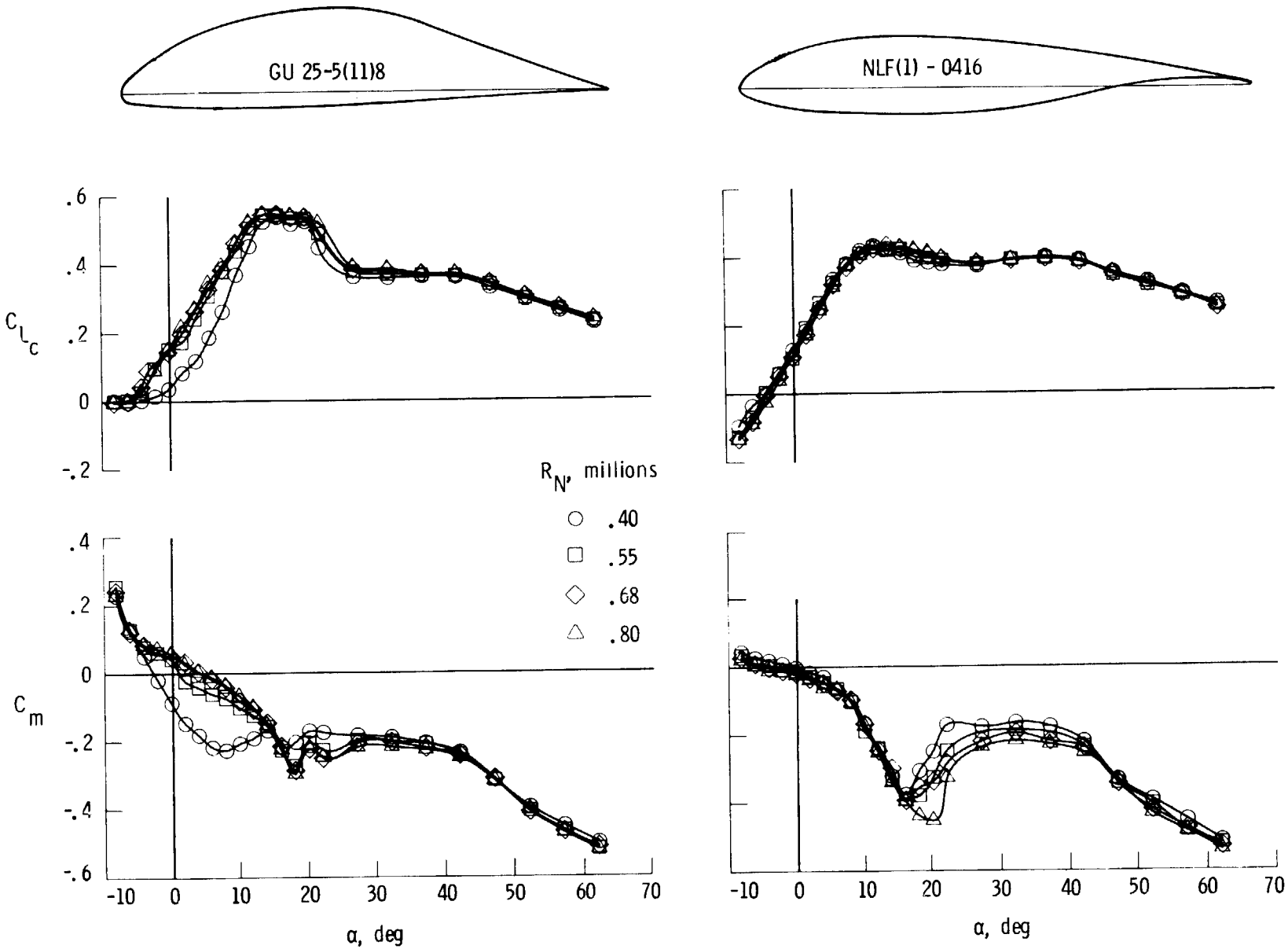

Figure 20.- Effect of Reynolds number on aerodynamic characteristics of canard, tractor configuration for two different canard airfoils.

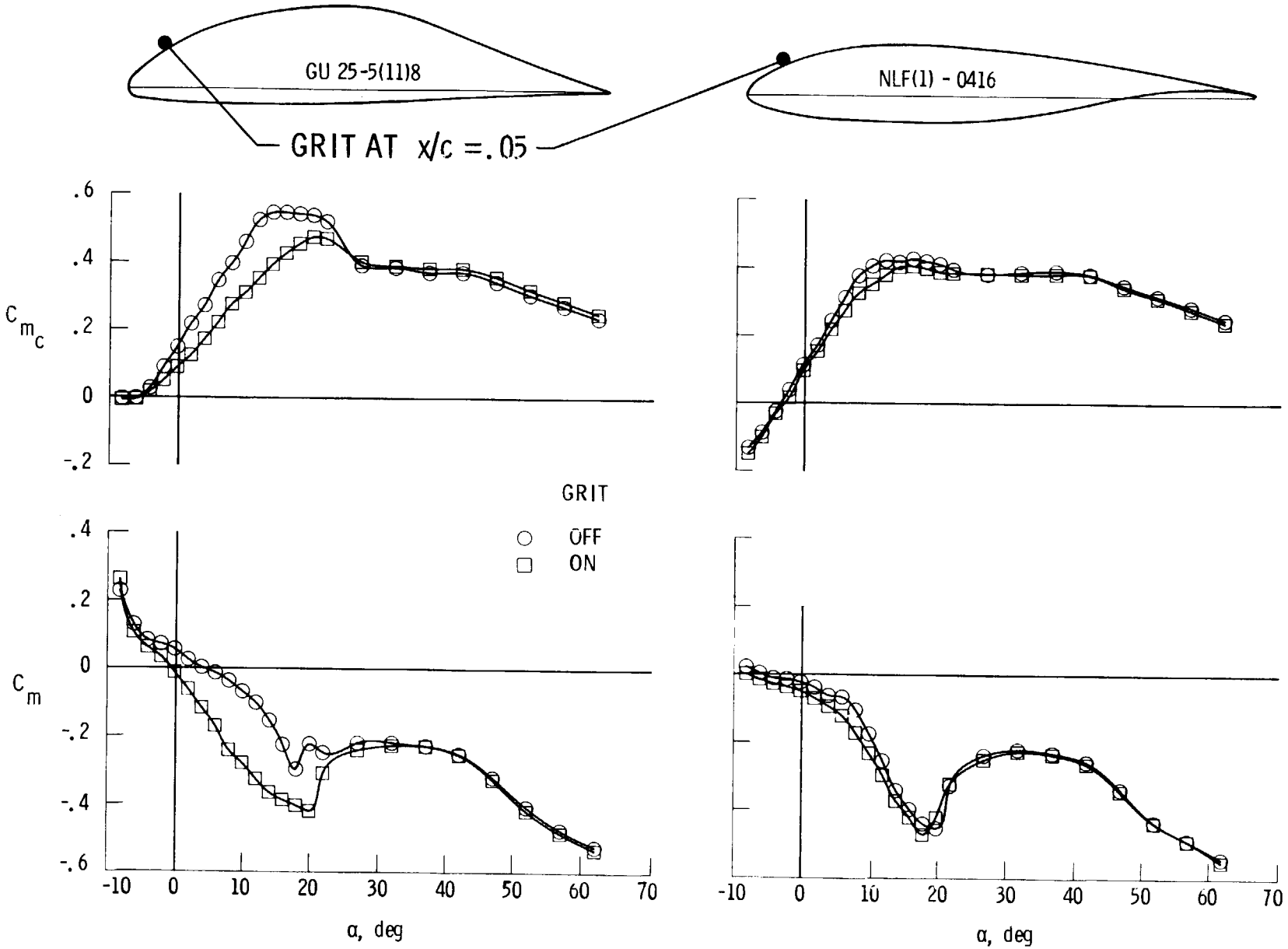

Figure 21.- Effects of fixed-transition on aerodynamic characteristics of canard, tractor configuration for two different canard airfoils. Reynolds number = 800,000.

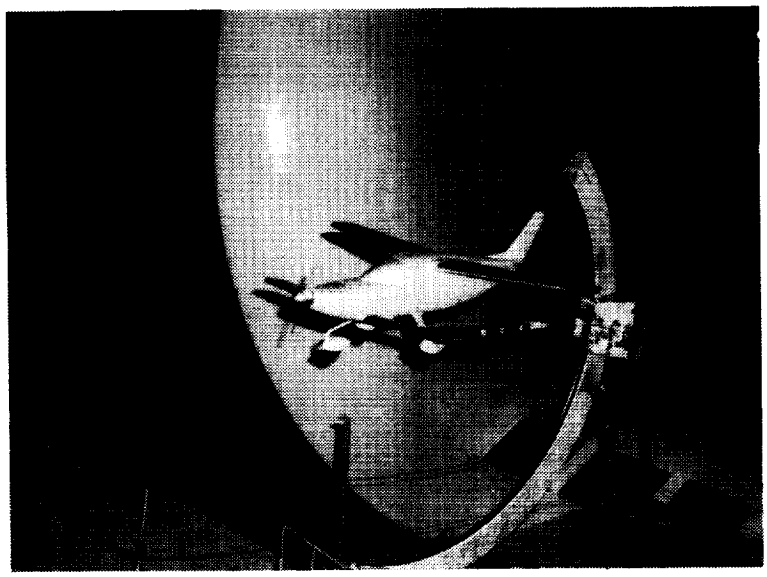

Figure 22.- High-wing, low-canard tractor configuration.

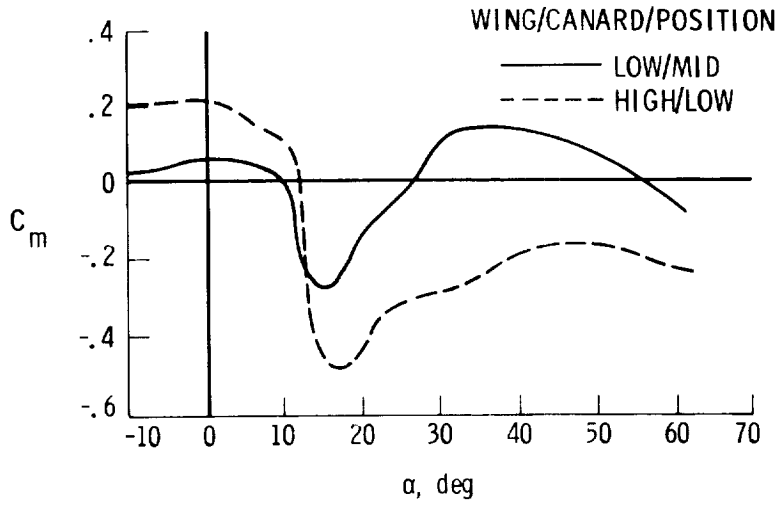

Figure 23.- Effect of canard/wing arrangement on pitching-moment characteristics of canard tractor design.

Figure 24.- Conventional airplanes used in stall/spin research.

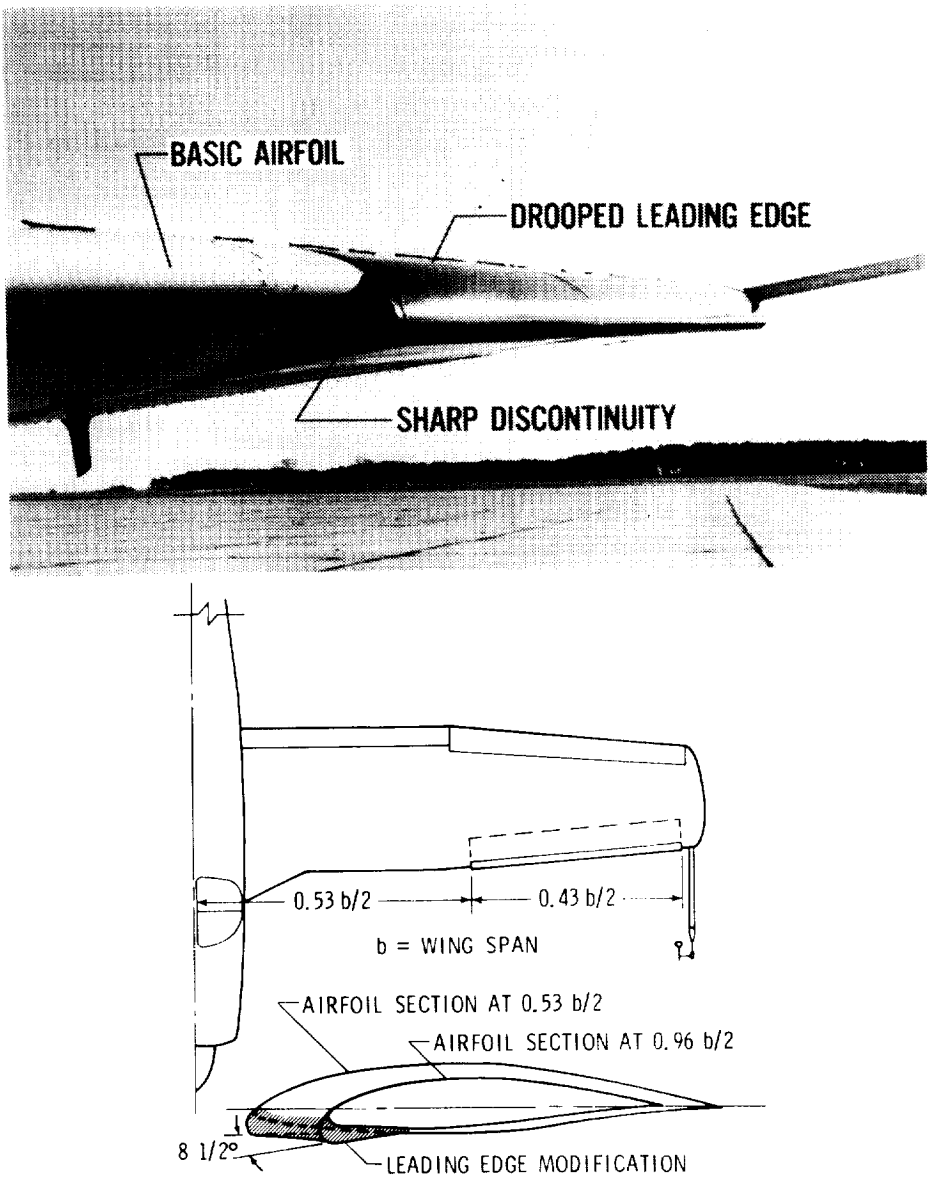

Figure 25.- Wing leading-edge droop used in stall/spin research.

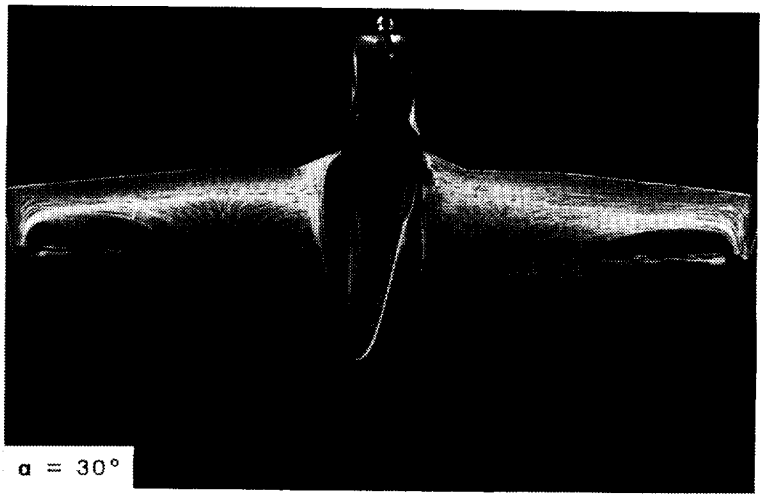

(a) Basic wing, $\alpha = 30°$.

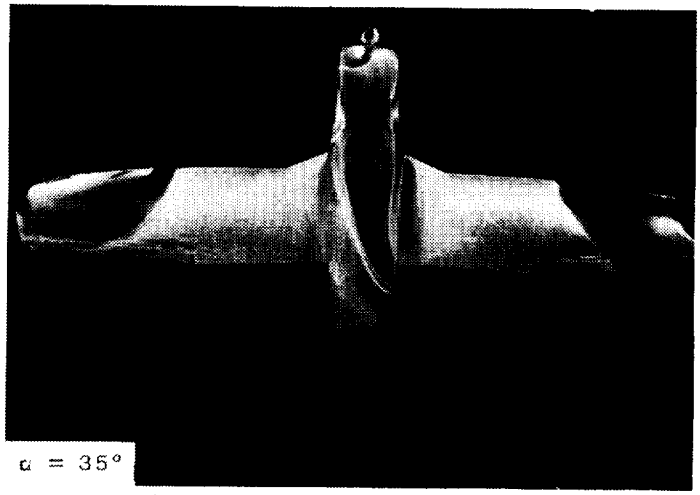

(b) Modified wing, $\alpha = 35°$.

Figure 26.- Oil flow visualization on tapered-wing model showing effect of leading-edge droop.

	NUMBER OF SPINS / ATTEMPTS	
	BASIC AIRPLANE	MODIFIED AIRPLANE
AA-1X (YANKEE)	$\frac{185}{193} = 96\%$	$\frac{0}{31} = 0\%$
C-23X (SUNDOWNER)	$\frac{127}{129} = 98\%$	$\frac{7}{134} = 5\%$
PA-28RX (ARROW)	$\frac{224}{255} = 88\%$	$\frac{12}{236} = 5\%$

Figure 27.- Summary of stall/spin flight test results showing spin resistance due to wing modifications.

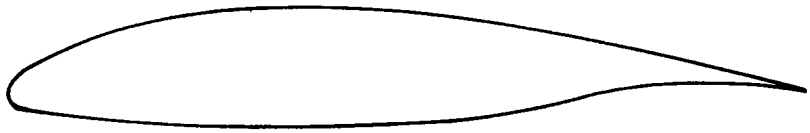

NLF(1)-0215 F (SOMERS)

NLF (1) - 0414 F (HARVEY/VIKEN)

Figure 28.- Sketch of two different airfoils designed for natural laminar flow.

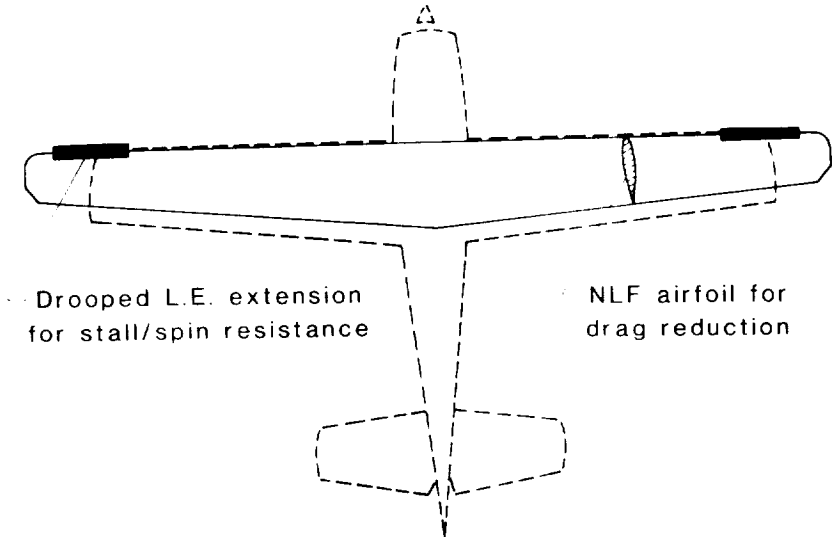

Figure 29.- Leading-edge droop modification applied to advanced wing design.

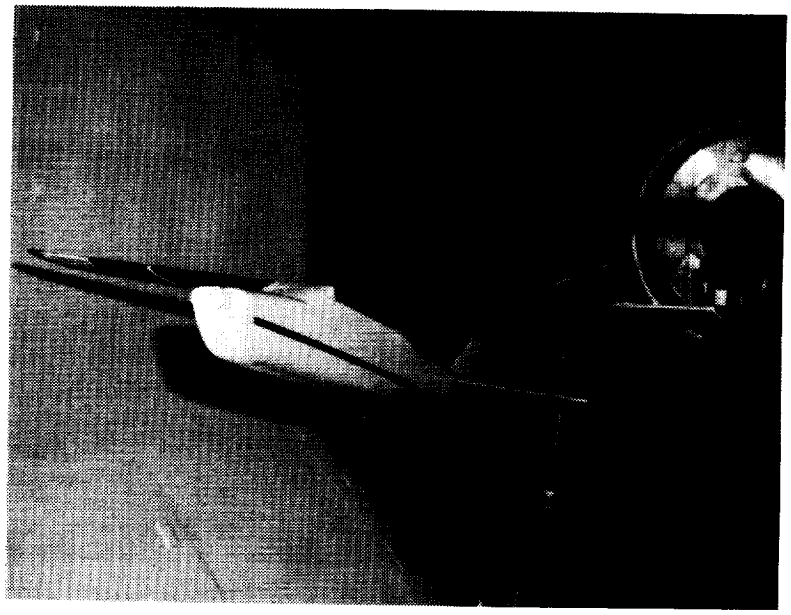

Figure 30.- Photograph of leading-edge droop on advanced wing design in Langley 12-Foot Low-Speed Wind Tunnel.

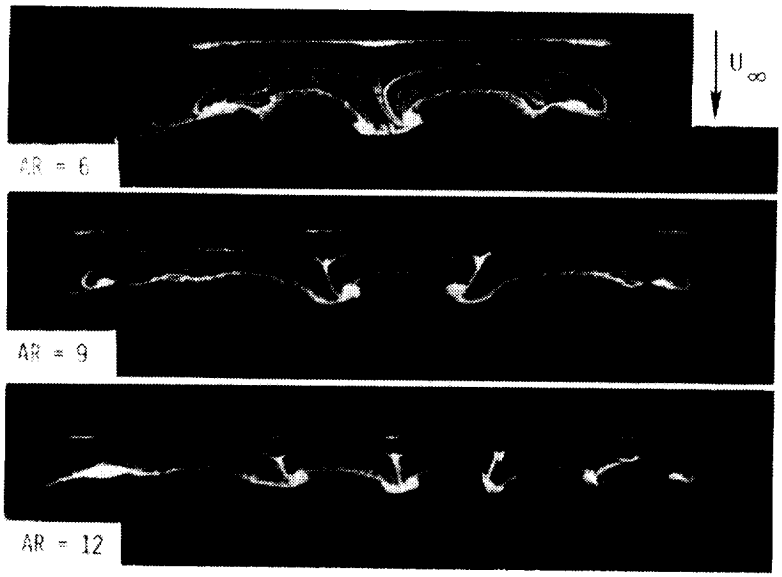

Figure 31.- Oil flow patterns developed on a series of wings (14% Clark Y airfoils of various aspect ratios, α = 18.4°, Reynolds number = 385,000.

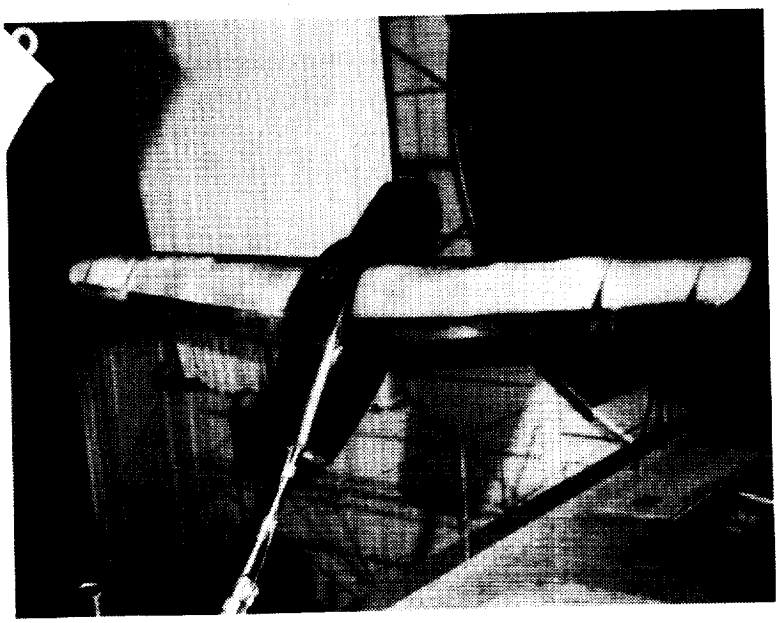

Figure 32.- Chemical sublimation study showing extent of natural laminar flow on advanced wing design.

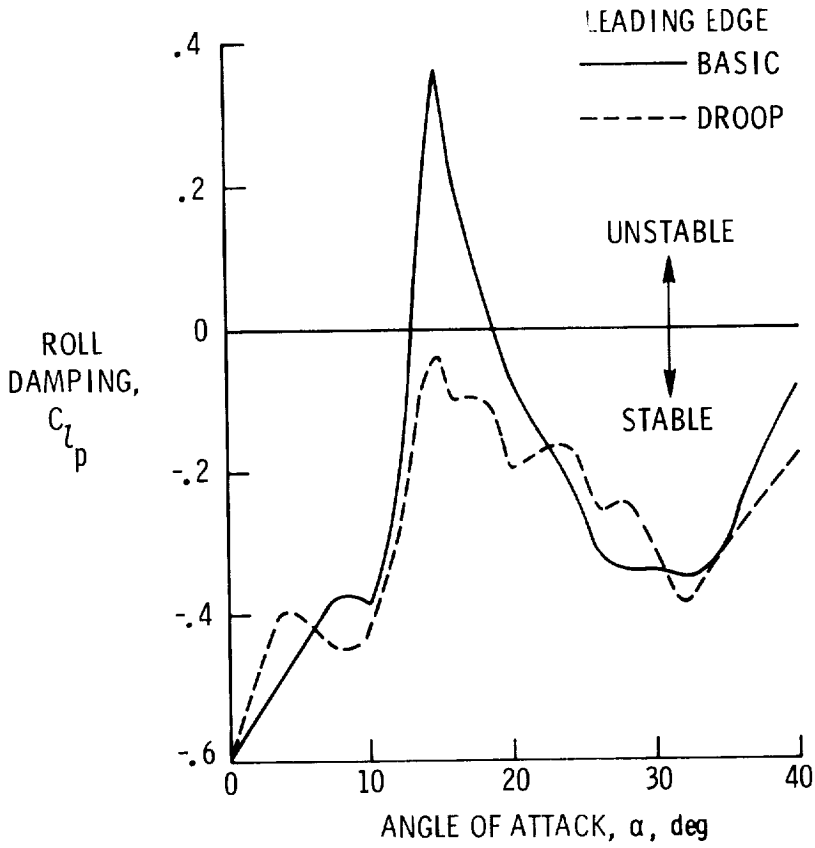

Figure 33.- Effect of leading-edge droop on roll damping characteristics of advanced wing design.

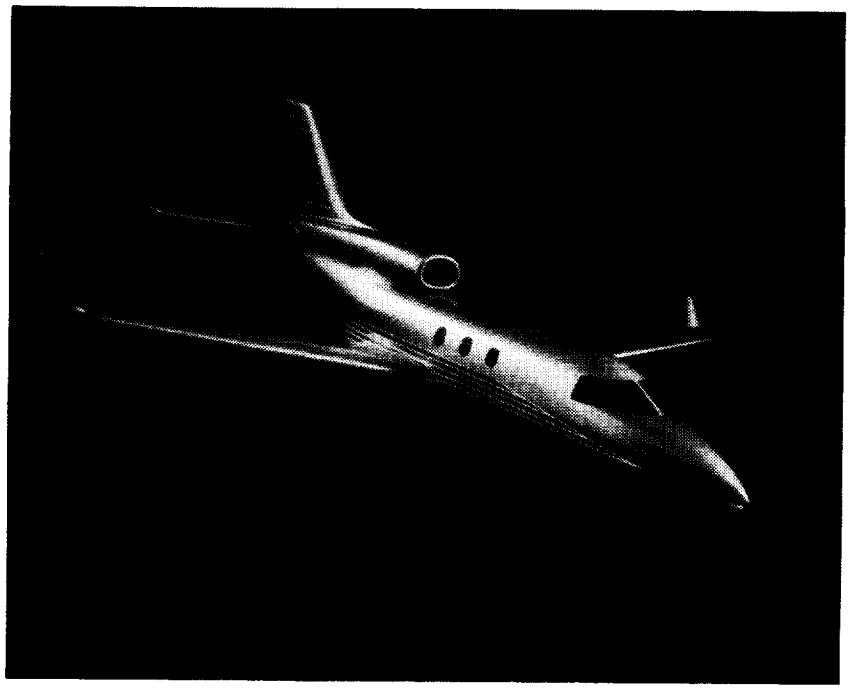

Figure 34.- Photograph of business jet configuration.

Figure 35.- Sketch of leading-edge droop design used on business jet configuration.

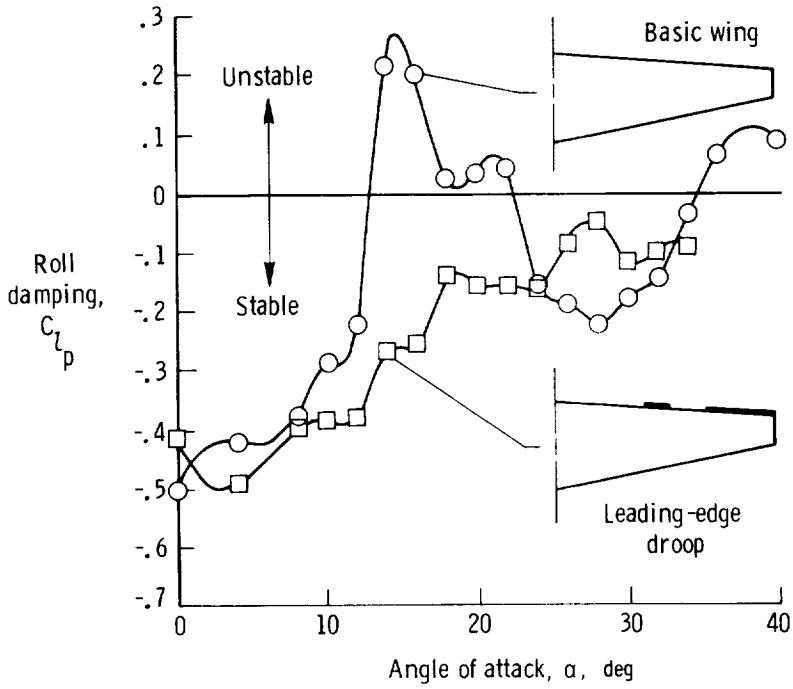

(a) Outboard droop alone.

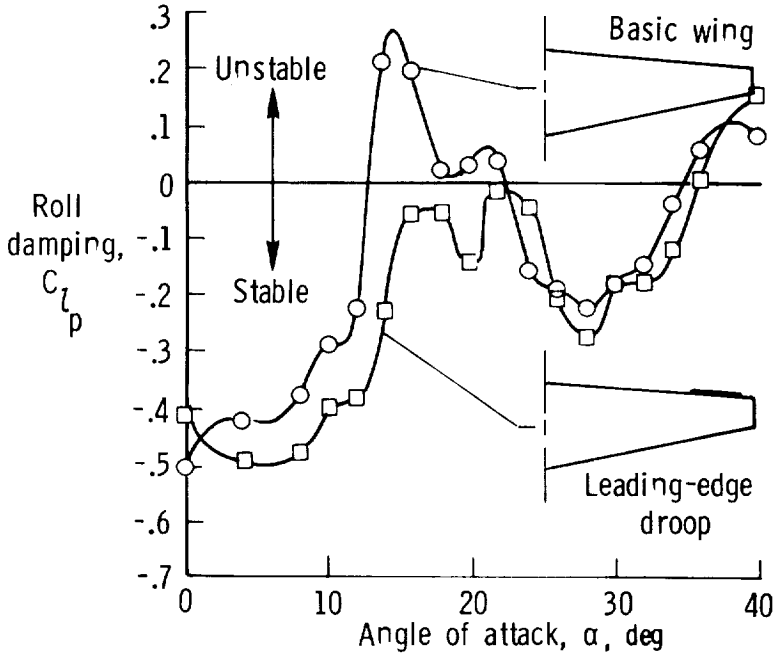

(b) Segmented droop.

Figure 36.- Effects of leading-edge droop on roll damping characteristics of business jet configuration.

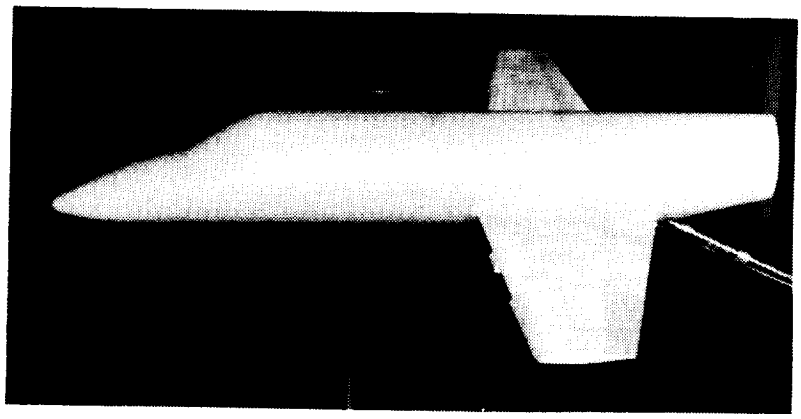

Figure 37.- Chemical sublimation studies on business jet in the 30- by 60-Foot Wind Tunnel.

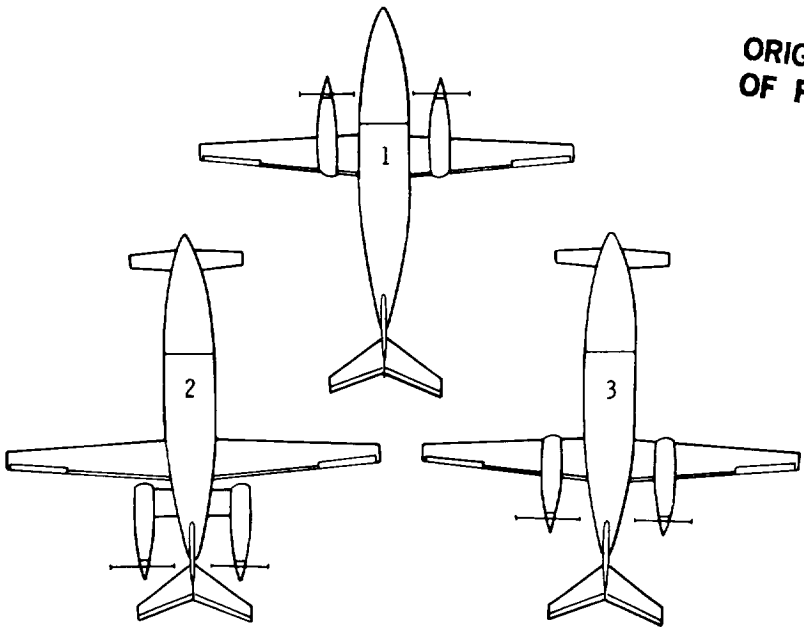

Figure 38.- Plan views of three-surface and conventional configurations.

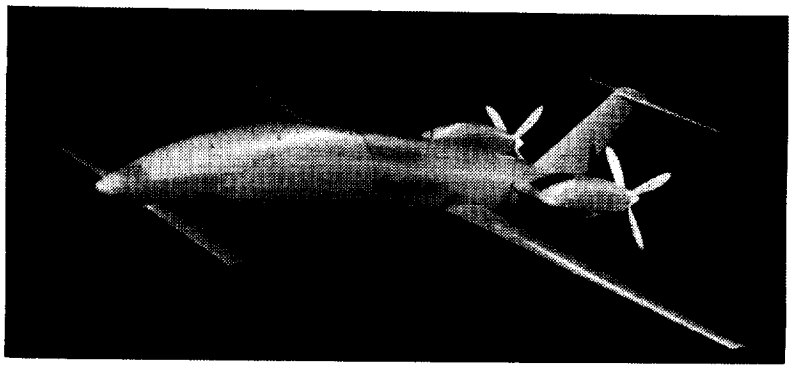

Figure 39.- Photograph of model of three-surface configuration.

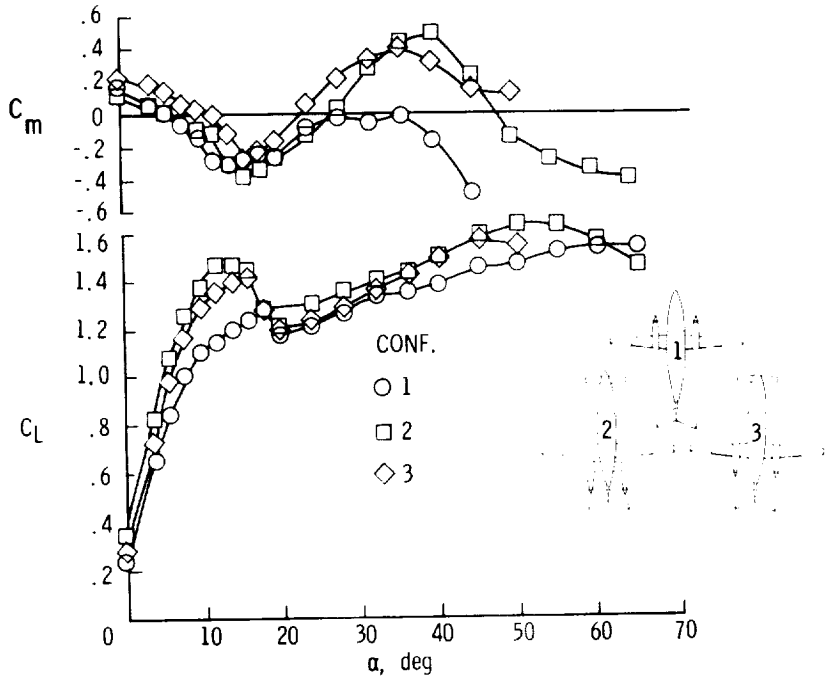

(a) Power off.

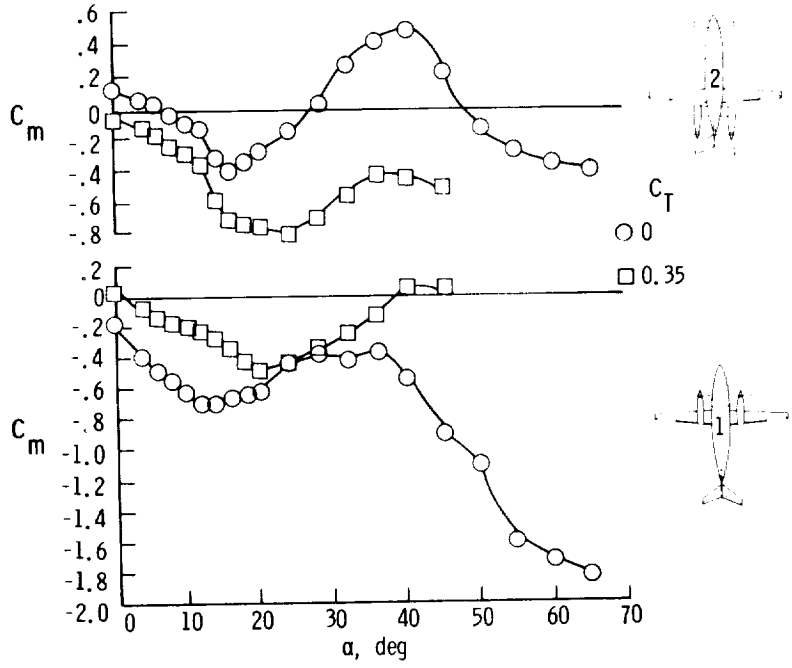

(b) Power on.

Figure 40.- Effects of power on longitudinal characteristics.

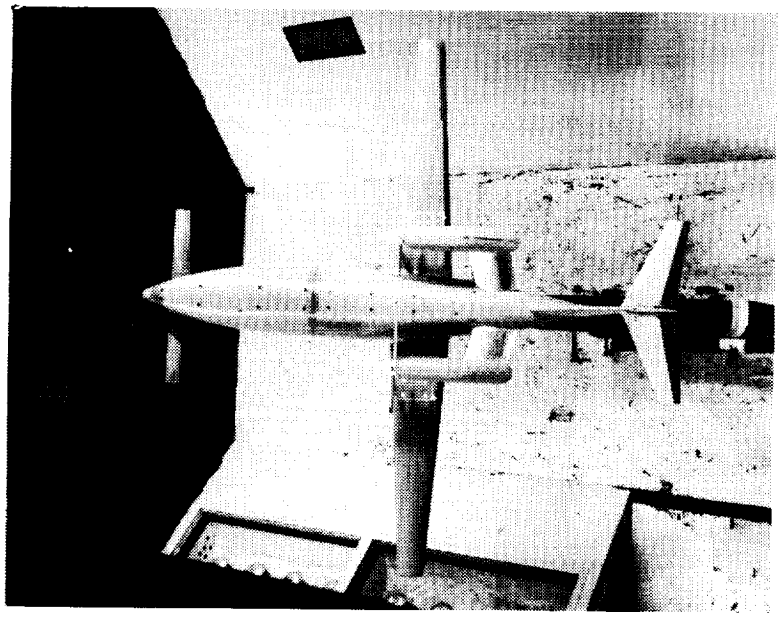

Figure 41.- Photograph of three-surface over-the-wing propeller configuration.

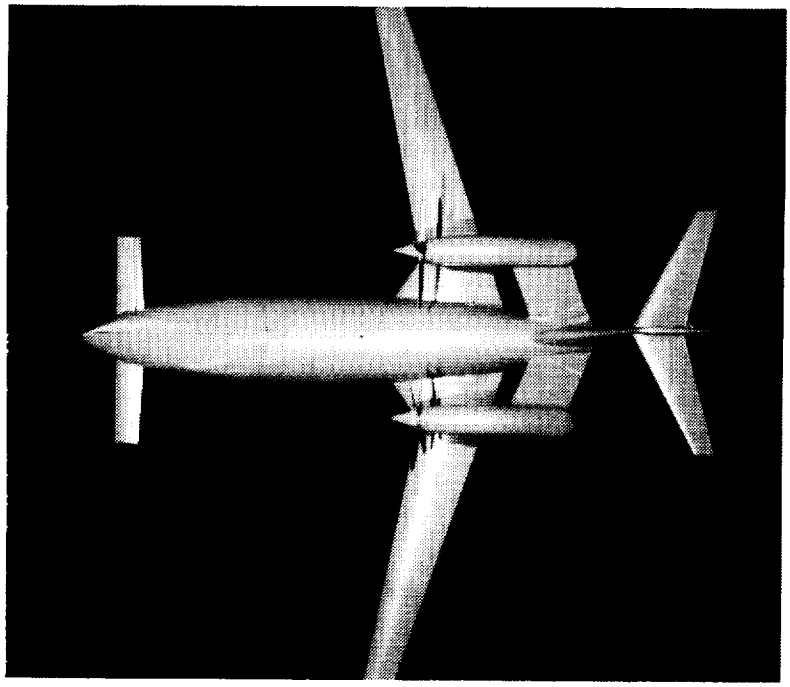

Figure 42.- Plan view photograph of three-surface over-the-wing propeller configuration with forward-swept wing.